

1 Explaining the large variability in empirical relationships between magnetic pore  
2 fabrics and pore space properties

3 Andrea R. Biedermann, Michele Puggetti, Yi Zhou

4 Institute of Geological Sciences, University of Bern, Baltzerstrasse 1+3, 3012 Bern, Switzerland

5  
6 Accepted date:

7 Received date: June 9<sup>th</sup>, 2021

8 in original form date: March 10<sup>th</sup>, 2021

9  
10  
11 Address for correspondence

12 Andrea R. Biedermann

13 Institute of Geological Sciences

14 University of Bern

15 Baltzerstrasse 1+3

16 3012 Bern

17 Switzerland

18  
19 andrea.regina.biedermann@gmail.com

20 Phone: +41 (0)31 631 4534

## Summary

The magnetic anisotropy exhibited by ferrofluid-impregnated samples serves as a proxy for their pore fabrics, and is therefore known as magnetic pore fabric. Empirically, the orientation of the maximum susceptibility indicates the average pore elongation direction, and predicts the preferred flow direction. Further, correlations exist between the degree and shape of magnetic anisotropy and the pores' axial ratio and shape, and between the degrees of magnetic and permeability anisotropies. Despite its potential, the method has been rarely used, likely because the large variability in reported empirical relationships compromises interpretation. Recent work identified an additional contribution of distribution anisotropy, related to the arrangement of the pores, and a strong dependence of anisotropy parameters on the ferrofluid type and concentration, partly explaining the variability. Here, an additional effect is shown; the effective susceptibility of the ferrofluid depends on the measurement frequency, so that the resulting anisotropy depends on measurement conditions. Using synthetic samples with known void geometry and ferrofluids with known susceptibility (4.04 SI and 1.38 SI for EMG705 and EMG909, respectively), magnetic measurements at frequencies from 500 Hz to 512 kHz are compared to numerical predictions. Measurements show a strong frequency-dependence, especially for EMG705, leading to large discrepancies between measured and calculated anisotropy degrees. We also observe artefacts related to the interaction of ferrofluid with its seal, and the aggregation of particles over time. The results presented here provide the basis for a robust and quantitative interpretation of magnetic pore fabrics in future studies, and allow for re-interpretation of previous results provided that the ferrofluid properties and measurement conditions are known. We recommend that experimental settings are selected to ensure a high intrinsic susceptibility of the fluid, and that the effective susceptibility of the fluid at measurement conditions is reported in future studies.

## Keywords

Magnetic fabrics and anisotropy  
Permeability and porosity  
Magnetic properties

## 1. Introduction

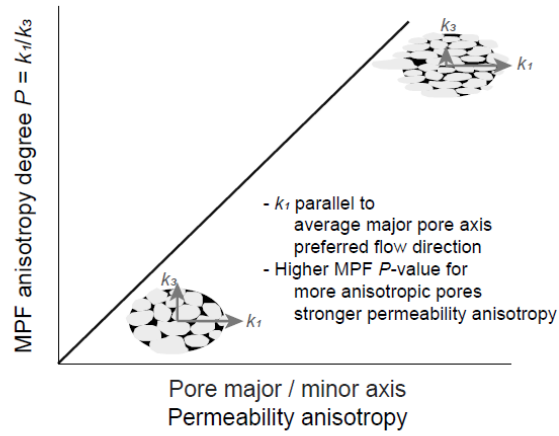
Magnetic pore fabrics (MPF) have been proposed as a fast and efficient way to characterize the anisotropy of pore space in rocks (Pfleiderer and Halls, 1990), and to predict permeability anisotropy and preferred flow directions (Pfleiderer and Halls, 1994, Hailwood *et al.*, 1999). They are defined as the anisotropy of magnetic susceptibility (AMS) of ferrofluid-impregnated samples, and may reflect depositional or tectonic fabrics (Pfleiderer and Kissel, 1994, Hailwood and Ding, 2000, Parés *et al.*, 2016). As pore fabrics control fluid flow in porous media, their accurate description is important in many areas of geophysics and geology, including convective flow models, aquifer and reservoir characterization, geothermal energy and CO<sub>2</sub> storage applications (Ayan *et al.*, 1994, Huang *et al.*, 2017, Ijeje *et al.*, 2019, Panja *et al.*, 2021, Sinan *et al.*, 2020, Wang *et al.*, 2014, Wang *et al.*, 2019, Willems *et al.*, 2017, Storesletten, 1998). Traditional pore characterization methods such as X-ray tomography face trade-offs between sample size and resolution, and generate large amounts of data that need to be processed (Cnudde and Boone, 2013, Landis and Keane, 2010). For applications that require characterization of the average pore fabric, MPFs provide a promising alternative in that they describe the average pore fabric as a single second-order tensor, measured on a representative sample volume, and potentially capturing pores down to 10 nm, without being affected by mineral and grain boundary properties unlike seismic anisotropy (Robion *et al.*, 2014, Almqvist *et al.*, 2011, Pfleiderer and Halls, 1990, Benson *et al.*, 2003).

Correlations between average pore axial ratio and MPFs have been proposed and investigated since the earliest MPF studies, using both natural and synthetic samples (Pfleiderer and Halls, 1990, Pfleiderer and Halls, 1993, Hrouda *et al.*, 2000, Jones *et al.*, 2006, Jezek and Hrouda, 2007, Nabawy *et al.*, 2009). Additionally, MPFs were compared to other measures of pore space anisotropy, e.g. anisotropy of elastic properties or electrical conductivity (Louis *et al.*, 2005, Robion *et al.*, 2014, Benson *et al.*, 2003, Nabawy *et al.*, 2009). Although reported empirical relationships for fabric orientation are similar for all studies (maximum susceptibility indicating the average pore elongation direction and maximum permeability), there is a large variability in reported relationships between

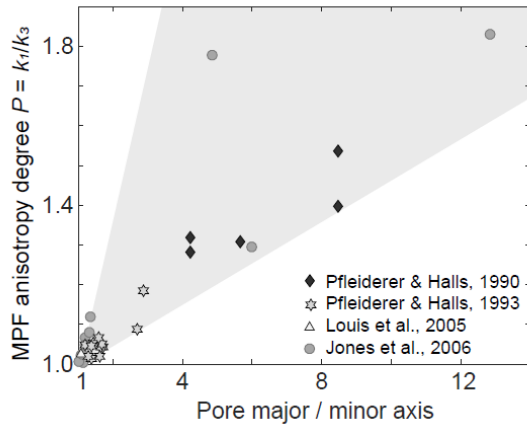
MPF anisotropy degree and pore aspect ratio or degree of permeability anisotropy (Fig. 1) (Pfleiderer and Halls, 1990, Pfleiderer and Halls, 1993, Pfleiderer and Halls, 1994, Louis *et al.*, 2005, Jones *et al.*, 2006, Nabawy *et al.*, 2009). Therefore, quantitative and robust interpretation of MPF data is not yet possible, and while the method is promising, it has been used rarely. For the method to become more widely applied, understanding the variability between reported empirical relationships is crucial, and the goal of this paper. The basis for interpreting the empirical relationships reported in rocks is to understand the fundamentals, and this is achieved here on synthetic samples with simple and known pore geometries.

One explanation for the large variability in empirical relationships is that different types of ferrofluids at different concentrations have been used when these relationships were established. In the meantime, it has become evident that for a given pore axial ratio, the MPF anisotropy degree increases nonlinearly with increasing fluid susceptibility (Biedermann, 2019, Jones *et al.*, 2006). The same applies to correlations with permeability anisotropy, which are further complicated by the fact that only few MPF studies report full permeability tensors based on six independent measurements (Pfleiderer and Halls, 1994, Hailwood *et al.*, 1999), whereas measurements along only two or three directions parallel to the macroscopic fabric are more common (Benson *et al.*, 2003, Louis *et al.*, 2005, Nabawy *et al.*, 2009). If the number of measurements is lower than that needed to define the full tensor, the calculated anisotropy underestimates the true anisotropy, unless the measurement directions coincide with the principal axes of the tensor.

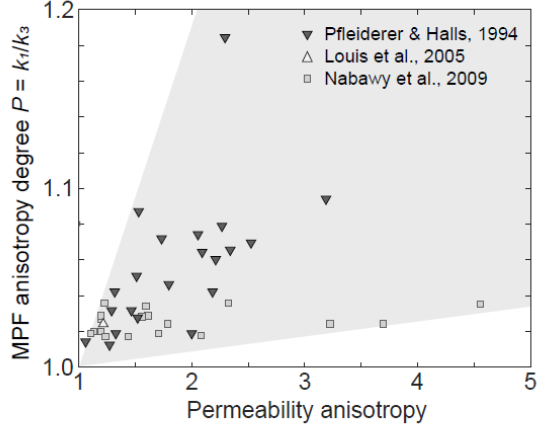
(a) Empirical relationships



(b) Literature data: MPF vs pore shape



(c) Literature data: MPF vs permeability



94

95 *Fig. 1: (a) Simplified empirical relationships between magnetic pore fabric (MPF) and average pore*  
 96 *alignment, or permeability anisotropy; (b,c) Literature data from which empirical relationships were*  
 97 *derived show large scatter.*

98

Secondly, the impregnation process and associated changes in the pore space properties may result in differences between studies. Two standard methods are used for impregnation, (1) evacuating the pore space under vacuum conditions and then supplying ferrofluid (Parés *et al.*, 2016, Pfeleiderer and Halls, 1990, Benson *et al.*, 2003, Robion *et al.*, 2014, Hrouda *et al.*, 2000), or (2) injecting the ferrofluid under pressure, which leads to different fabrics depending on the injection pressure (Esteban *et al.*, 2006). It is not clear, however, whether this is related to smaller pores being impregnated at higher pressure, or the destruction of pore walls during impregnation. Additional impregnation methods are being tested (Pugnetti *et al.*, 2021).

A third reason for the variability is that the MPF data has been largely compared to the average pore axial ratio, shape and orientation, i.e., assuming that MPFs are controlled by shape anisotropy (Pfeleiderer and Halls, 1990, 1993, Hrouda *et al.*, 2000, Jones *et al.*, 2006, Jezek and Hrouda, 2007).

Shape anisotropy results from self-demagnetization, a process that occurs when a strongly magnetic body with a high intrinsic susceptibility  $k_{int}$  (e.g., an ore body, magnetite grain, or ferrofluid-filled pore) is surrounded by weakly magnetic material (e.g., rock) (Clark and Emerson, 1999). Self-demagnetization reduces the observed susceptibility  $k_{obs}$  to  $k_{obs} = (I + k_{int}N)^{-1}k_{int}$ , where  $I$  is the unit matrix, and  $N$  the self-demagnetization tensor, which depends on the shape of the strongly magnetic body (e.g. Clark, 2014). It can be easily calculated for ellipsoids (Osborn, 1945, Stoner, 1945), and approximated for other simple body shapes (Sato and Ishii, 1989, Joseph, 1966, Joseph, 1967). However, self-demagnetization tensors may change throughout a body of complex shape (Joseph, 1976, Joseph and Schlömann, 1965). In addition to the shape preferred orientation of single pores, also their arrangement controls the measured MPF. Rocks contain numerous pores in a complex and irregular three-dimensional network, and distribution anisotropy, arising from magnetostatic interaction of the ferrofluid in different pores, also contributes to the measured anisotropy (Biedermann, 2019, Biedermann, 2020). Distribution anisotropy has been extensively investigated for magnetite grains in rocks (Grégoire *et al.*, 1998, Grégoire *et al.*, 1995, Hargraves *et al.*, 1991, Cañón-Tapia, 1996, Cañón-Tapia, 2001, Stephenson, 1994), and is described in a similar

way for MPFs (Biedermann, 2019, Biedermann, 2020). Thus, the MPF depends not only on the pores' shape preferred orientation as proposed initially, but also on the distribution of the pores throughout the rock. The mathematical treatment of distribution anisotropy in MPF studies relies on the assumption that the fluid susceptibility is homogeneous throughout the pore space, and that impregnated pores possess similar magnetic properties to solid grains of the same susceptibility. Recent work is testing these models by comparing measured MPFs to predictions based on pore characterization using X-ray microtomography (Zhou *et al.*, 2021).

Finally, measurement conditions, specifically frequency, may affect MPF results. Ferrofluids are colloidal suspensions of magnetic nanoparticles in non-magnetic water- or oil-based carrier fluid. The nanoparticles are coated with surfactant to avoid agglomeration, and their size of ~10 nm ensures they are kept in suspension by Brownian motion (Odenbach, 2004, Joseph and Mathew, 2014, Torres-Diaz and Rinaldi, 2014, Rosensweig, 1987, Rosensweig, 1988, Papaefthymiou, 2009). Magnetite particles in this size range behave superparamagnetically at room temperature, and their susceptibility is frequency-dependent (Söffge and Schmidbauer, 1981, Muscas *et al.*, 2013, Néel, 1949, Bean and Livingston, 1959, Brown, 1959, Stephenson, 1971, Dormann, 1981, Jones and Srivastava, 1989, Coffey and Kalmykov, 2012). This characteristic is exploited in environmental magnetism, where frequency-dependence of susceptibility is used to infer grain size distributions (Dearing *et al.*, 1996, Eyre, 1997, Worm, 1998, Worm and Jackson, 1999, Hrouda, 2011). Out-of-phase susceptibility is a second property related to frequency dependence, and also used for magnetic granulometry (Hrouda *et al.*, 2013). Other possible sources of frequency-dependence and out-of-phase susceptibility are eddy currents or low-field hysteresis, observed in pyrrhotite and Ti-magnetite (Jackson, 2003-2004, Kostrov *et al.*, 2018, Hrouda *et al.*, 2013, Jackson *et al.*, 1998). Physical motion of particles in response to the magnetic field may play an additional role (Brown, 1959, Brown, 1963, Dormann, 1981). Brownian motion is constrained by the pore walls, and may be restricted in certain pores due to their size. If this affects frequency dependence, it may help to distinguish between fabrics of different pore size fractions. Frequency-dependent properties and

out-of-phase susceptibility are thus expected for the ferrofluid used in MPF studies. Of particular interest here is whether the frequency-dependence of susceptibility also affects the anisotropy. One indication that this may be the case is a large variability in effective anisotropy constants of magnetite nanoparticles depending on whether the measurements were obtained in DC or AC fields (Goya *et al.*, 2003). Unfortunately, neither the intrinsic susceptibility of the fluid, nor the measurement frequency have been reported in most MPF studies. Even though the frequency can sometimes be estimated from the instrument used, the lack of information on fluid susceptibility makes it impossible to compare results and empirical relationships between studies. Thus frequency-dependence and its potential effect on anisotropy and MPF interpretations remain to be investigated.

This study characterizes MPFs and their frequency dependence in synthetic samples with a range of pore sizes, aspect ratios, and arrangements. Measurements obtained at a range of frequencies are compared to numerical models taking into account shape and distribution anisotropy. Models are based on the initial susceptibilities given in the fluids' technical specifications. Differences between expected and effective susceptibilities and related discrepancies between models and measurements are discussed. The term 'expected susceptibility' is used here to describe the susceptibility calculated from the initial susceptibility and shape of the fluid-filled void. 'Effective susceptibility' is used to describe the actually measured susceptibility. Both expected and effective susceptibilities refer to observables and are affected by self-demagnetization, i.e., they depend on the shape of the void. They should be equal if the intrinsic susceptibility of the fluid at measurement conditions equals the initial susceptibility reported in the fluid's technical specifications. A major finding of this work is the strong decrease of effective ferrofluid susceptibility with frequency, in particular for water-based ferrofluid EMG705, with important consequences for the interpretation of MPFs. The experiments shown here also identify difficulties and unwanted effects that may complicate the interpretation of MPFs in rocks.



## 2. Material and Methods

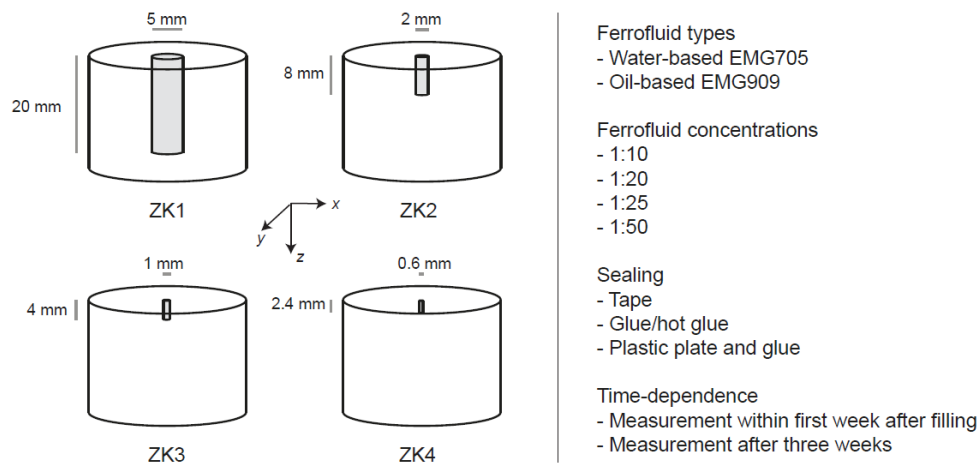
### 2.1 Samples

Two sets of samples have been prepared for this study. The first group (label prefix ZK) contains one cylindrical pore with a ratio diameter:height equal to 1:4, and four different sizes, defined by cylinder diameters of 0.6 – 5 mm. In the second group (label D.T., where the number after D indicates the diameter, and the number after T the cylinder height), each sample contains a set of 9 cylindrical pores, with different samples having diameter:height ratios of 1:2, 1:4 and 1:8, and diameters of 0.5 mm, 1 mm, and 2 mm (Fig. 2). The ZK sample group was used to investigate the effects of ferrofluid type and concentration, as well as testing different types of sealing. The anisotropy parameters of the four different sizes should in theory be equal for the same ferrofluid and concentration, so that these samples allow to investigate size-dependent effects. Conversely, the main purpose of the D.T. samples is to investigate the interplay of shape and distribution anisotropies for different configurations of filled pores. Therefore, MPFs on the D.T. sample series were measured using a single ferrofluid and a single concentration.

The ZK samples were prepared from a 1-inch diameter polycarbonate cylinder, using an HSS/CNC drill at the Institute of Geological Sciences, University of Bern. The samples were prepared such that the diameter:height ratio and the expected MPF is the same for all samples, although the void volume and therefore mean susceptibility are different. The volume-effect can be removed by normalizing all magnetic data by the ferrofluid volume rather than the sample volume. Initially, eight sets of samples comprising four sizes each were drilled. These were filled with water- and oil-based ferrofluids, EMG705 and EMG909, respectively, at 1:10, 1:20, 1:25 and 1:50 volume concentrations of ferrofluid to carrier liquid. Attempts to dilute the ferrofluids at a ratio 1:100, as used in Parés *et al.* (2016), failed due to aggregation of the particles, and their precipitation before the fluid could be filled into the samples. The initial susceptibilities of EMG705 and EMG909 are reported as 4.04 (SI) and 1.38 (SI) (EMG 705 Specifications and Physical Properties; <https://ferrofluid.ferrotec.com/products/ferrofluid-emg/water/emg-705/> and EMG909

Specifications and Physical Properties <https://ferrofluid.ferrotec.com/products/ferrofluid-emg/oil/emg-909/>). The measured susceptibilities of the carrier fluids are  $-1.0(\pm 0.1) \cdot 10^{-5}$  and  $-1.6(\pm 0.1) \cdot 10^{-5}$  (SI) for water and oil respectively, orders of magnitude lower than those of the ferrofluid, and thus negligible. The diluted ferrofluids have nominal intrinsic susceptibilities ranging from 0.03 to 0.4 (SI).

(a) ZK samples: single pore, constant ratio major/minor axis (4:1), four sizes - effect of ferrofluid type and concentration



(b) D.T. samples: multiple pores, three aspect ratios and sizes - effect of distribution anisotropy and impregnation efficiency

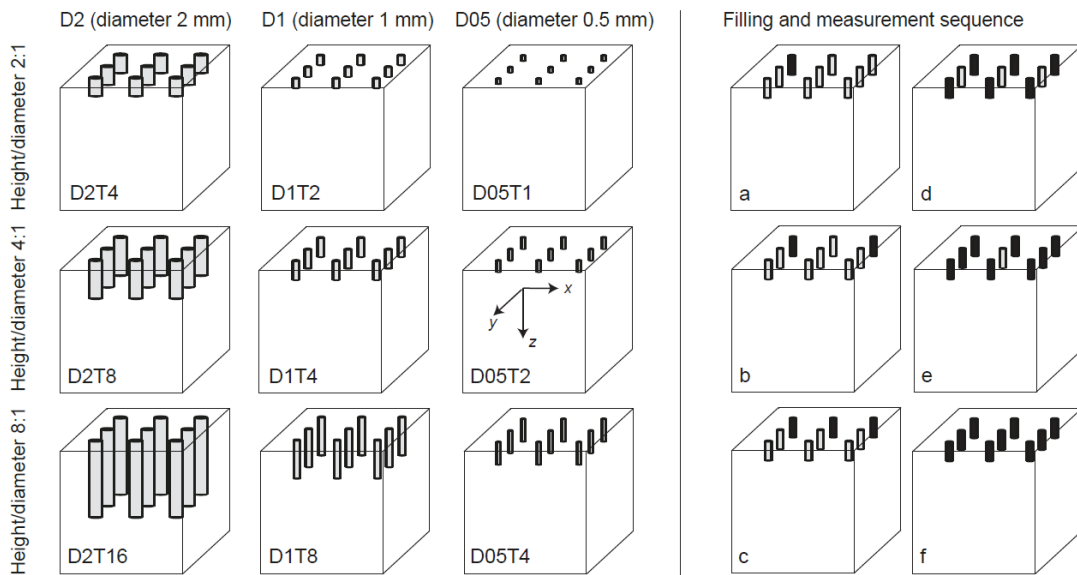


*Fig. 2: Pore dimensions and assemblies of filled pores for the studied samples. The scientific questions addressed with each sample group were different: (a) ZK samples served the purpose of investigating the influence of ferrofluid properties and sample preparation; (b) the D.T. samples allowed to characterize the effects of pore shape and arrangement.*

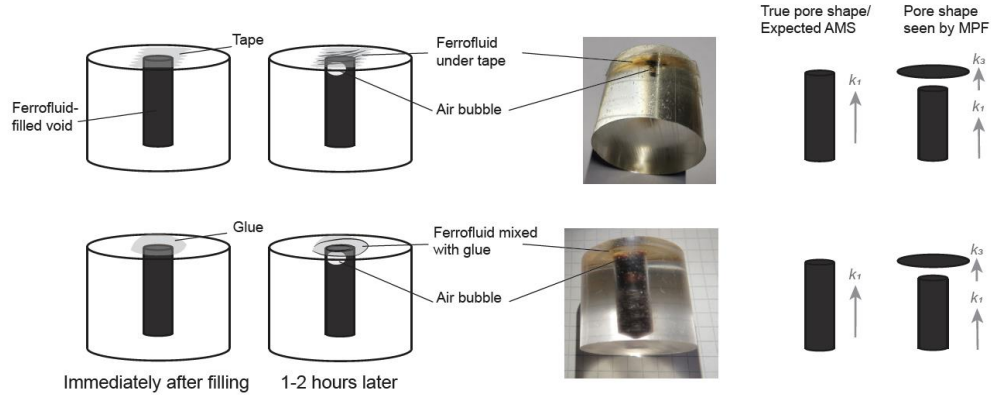
213 Prior to MPF measurements, each void was sealed with different materials, including tape or various  
214 kinds of glue. Sealing with tape was unsuccessful, because it was hardly possible to prevent the  
215 formation of air bubbles, and because the fluid migrated into the space between the cylinder surface  
216 and the tape, likely due to capillary forces, over timespans of hours. Glued seals showed mixing  
217 artefacts, i.e., a small portion of the ferrofluid would diffuse into the glue while the glue was drying  
218 (Fig. 3). This was particularly problematic for oil-based ferrofluid and the largest voids, which  
219 required most glue and therefore long drying times. Additionally, oil-based ferrofluid would react  
220 with the glue and destroy its sealing capacities over timeframes of a few days.

221 A second set of ZK samples was then drilled, and these were filled with special care to prevent air  
222 bubbles or diffusion of ferrofluid outside the void. To achieve this, the voids were sealed with hot  
223 glue that dries faster than normal glue thus minimizing interaction with ferrofluid, and a  
224 combination of hot glue with a plastic plate containing two smaller holes to allow exchange of air  
225 during filling and sealing, while at the same time reducing the amount of glue and drying time.  
226 Despite all precautions taken, trapped air could not be avoided completely, and in all samples, air  
227 bubbles appeared to develop over time.

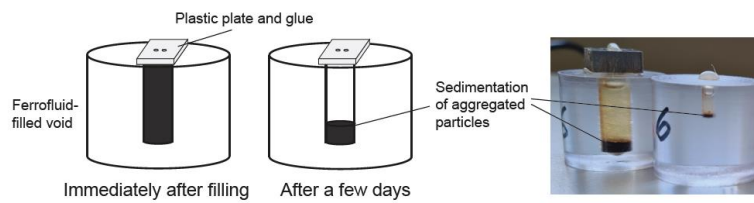
228 The D.T. samples were prepared from polycarbonate, using CNC milling machines at the Physics  
229 Institute, University of Bern. A total of nine cubic samples were made, with three aspect ratios  
230 (diameter:height ratios of 1:2, 1:4 and 1:8), and three sizes (2 mm, 1 mm and 0.5 mm diameter). 3x3  
231 voids were drilled in a single face of the cube, at 8 mm distance from each other. To reduce the  
232 number of samples that needed to be prepared, the voids of each sample were filled sequentially,  
233 measuring the MPF before filling the next void(s). This procedure allowed to obtain six datasets from  
234 each of the nine samples. Based on the experience with the ZK samples, water-based EMG705  
235 ferrofluid diluted with distilled water at 1:10 was used to fill the voids, and hot glue for sealing.  
236 Water-based fluid is less prone to particle aggregation and sedimentation, and interacts less with  
237 glue than oil-based fluid, and this stability over time was important for the chosen sequence of filling

238 and measuring the different sets of voids one after the other. A lower-case letter at the end of the  
 239 sample name indicates the pattern of filled voids.

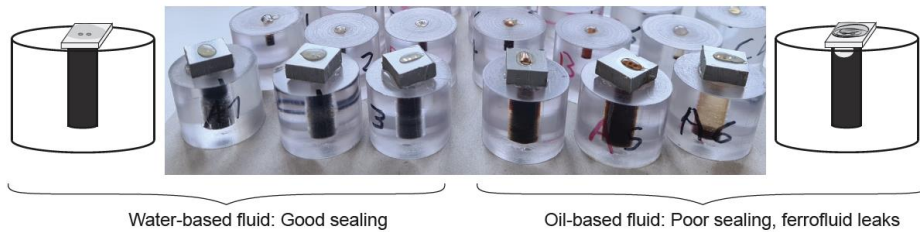
(a) Sample preparation and preparation-related artefacts: Interaction of ferrofluid and seal



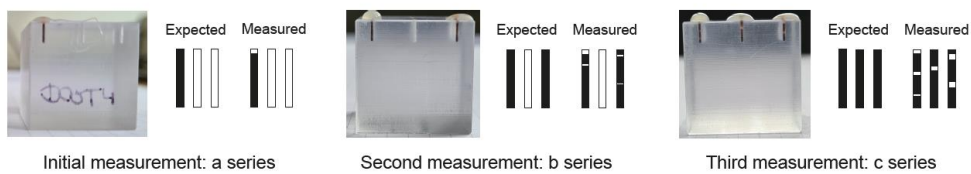
(b) Sample preparation and preparation-related artefacts: Nanoparticle aggregation and sedimentation



(c) Changes in sealing capabilities three weeks after sample preparation



(d) Changes in fluid configuration over time



240

241 *Fig. 3: Sample preparation and preparation-related artefacts: Conceptual sketches, pictures, and*  
 242 *influence on measured anisotropy for (a) migration of ferrofluid along the sample-seal interface or*  
 243 *mixing of ferrofluid with seal and formation of air bubbles; (b) particle aggregation and*  
 244 *sedimentation over time. (c) Changes in sealing capabilities three weeks after sample preparation,*  
 245 *resulting in ferrofluid leakage for oil-based EMG909; and (d) changes in fluid configuration over time,*  
 246 *affecting interpreted pore shapes.*

All voids have been drilled from a single side of the sample, to simplify the manufacturing process, resulting in asymmetric positioning of the void(s) within the cylinder or cube. A possible effect of the sample asymmetry on the measured anisotropy was tested by repeat measurements with slightly different sample positions. For the MFK1-FA, susceptibility measurements were independent of sample position, indicating that the field inside the coil of the MFK1-FA is homogeneous on the scale of the sample size and position variation. The large noise level of the SM150H/L instruments for repeat measurements with a given sample positioning outweighs any potential variation resulting from changes in sample positioning. Hence, the sample asymmetry does not affect the measured susceptibilities.

## 2.2 Expected magnetic properties

The expected magnetic properties for the configurations shown in Fig. 2 were calculated based on the known initial susceptibilities for the respective ferrofluid and its concentration, and the known pore shape, as well as the pore arrangement in the case of the D.T. samples.

Each of the ZK samples contains a single ferrofluid-filled cylindrical void with equal diameter/height ratio, so that their anisotropies are defined solely by shape anisotropy, and the demagnetization tensor is the same for each of them. Due to the sample geometry, the maximum susceptibility is expected along the z axis (cylinder axis), and there is a minimum susceptibility plane normal to that axis. The self-demagnetization factors along the three sample axes are  $N_x = N_y > N_z$ , and using the equation for cylinders given by Sato and Ishii (1989),  $N_x = N_y = 0.450$  and  $N_z = 0.0997$ . Had an ellipsoidal approximation been used (Osborn, 1945), the self-demagnetization factors would have been  $N_x = N_y = 0.462$ ,  $N_z = 0.0754$ . Expectations of the observed directional susceptibilities depend on the self-demagnetization tensor and fluid susceptibility, and the same is true for the expected anisotropy parameters (Table 1, Fig. 4a). The susceptibility anisotropy is described by the directional susceptibilities  $k_x$ ,  $k_y$ , and  $k_z$ , and their ratios. Additionally, the anisotropy degree  $P = \max(k_x, k_y, k_z) / \min(k_x, k_y, k_z)$  and anisotropy shape  $U = (2 * \text{median}(k_x, k_y, k_z) - \max(k_x, k_y, k_z) - \min(k_x, k_y, k_z)) / (\max(k_x, k_y, k_z) - \min(k_x, k_y, k_z))$  were used, analogously to  $P$  and  $U$  calculated from the

eigenvalues of the susceptibility tensor (Jelinek, 1981). Note that we are not using the standard notation in these equations, because  $P$  and  $U$  are defined based on the eigenvalues, and with only three directional measurements, it is in general not possible to define the full tensor nor its eigenvalues. Nevertheless, given the symmetry of the samples,  $k_x$ ,  $k_y$  and  $k_z$  are measured parallel to the expected principal susceptibility directions, and thus represent the eigenvalues.

All D.T. samples apart from the (a) series possess both shape and distribution anisotropy, and their expected directional susceptibilities were computed using the FinlrrSDA code (Biedermann, 2020). Because the spacing between the voids is constant for all samples, independent of void size, the distribution anisotropy contribution leads to different total anisotropies even when the shape anisotropies are the same (Table 1). For the (a) series, the anisotropy is equivalent to that expected for the ZK samples in that  $k_z > k_x = k_y$ . Interactions lead to a slight increase of  $k_x$  compared to  $k_y$  in the (b), (c) and (d) series, also affecting the shape of the anisotropy. For the configurations of these samples, the  $P$ -values are mainly defined by the aspect ratios of each void, while the distribution anisotropy has a smaller effect on the  $P$ -value, but largely affects the anisotropy shape  $U$  (Fig. 4b).

### 2.3 Magnetic measurements

The magnetic properties of the ZK samples had been measured prior to preparing the D.T. samples, and the results obtained for the ZK sample series were used the select suitable preparation and measurement sequences for the D.T. sample series. Therefore, the experiments performed on each series differ from each other.

**Table 1: Expected magnetic properties for the ZK (a) and D.T. (b) sample series. Directional susceptibilities ( $k_x$ ,  $k_y$ ,  $k_z$ ) normalized by ferrofluid volume, and anisotropy indicated by ratios of directional susceptibilities, anisotropy degree, and anisotropy shape. Initial susceptibilities: 4.04 (SI) for water-based EMG705, and 1.38 (SI) for oil-based EMG909.**

a) Expected susceptibility (normalized by ferrofluid volume) for ZK samples										
	Ferrofluid concentration	Void diameter:height	Magnetic pore fabric parameters							
			$k_x$	$k_y$	$k_z$	$y/x$	$z/x$	$z/y$	P	U
water-based ferrc	1:10	1:4	0.315	0.315	0.354	1.000	1.124	1.124	1.124	-1.000
	1:20	1:4	0.177	0.177	0.189	1.000	1.066	1.066	1.066	-1.000
	1:25	1:4	0.145	0.145	0.153	1.000	1.054	1.054	1.054	-1.000
	1:50	1:4	0.076	0.076	0.079	1.000	1.028	1.028	1.028	-1.000
oil-based ferroflu	1:10	1:4	0.119	0.119	0.124	1.000	1.043	1.043	1.043	-1.000
	1:20	1:4	0.064	0.064	0.065	1.000	1.023	1.023	1.023	-1.000
	1:25	1:4	0.052	0.052	0.053	1.000	1.019	1.019	1.019	-1.000
	1:50	1:4	0.027	0.027	0.027	1.000	1.009	1.009	1.009	-1.000
b) Expected susceptibility (normalized by ferrofluid volume) for D.T. samples (water-based fluid)										
	Ferrofluid concentration	Void diameter:height	Magnetic pore fabric parameters							
			$k_x$	$k_y$	$k_z$	$y/x$	$z/x$	$z/y$	P	U
a series (all)	1:10	1:2	0.319	0.319	0.344	1.000	1.078	1.078	1.078	-1.000
	1:10	1:4	0.315	0.315	0.354	1.000	1.124	1.124	1.124	-1.000
	1:10	1:8	0.313	0.313	0.360	1.000	1.152	1.152	1.152	-1.000
b series, D2	1:10	1:2	0.319	0.319	0.344	1.000	1.078	1.078	1.078	-0.994
	1:10	1:4	0.315	0.315	0.354	1.000	1.124	1.124	1.124	-0.993
	1:10	1:8	0.313	0.313	0.360	0.999	1.151	1.152	1.151	-0.988
b series, D1	1:10	1:2	0.319	0.319	0.344	1.000	1.078	1.078	1.078	-0.999
	1:10	1:4	0.315	0.315	0.354	1.000	1.124	1.124	1.124	-0.999
	1:10	1:8	0.313	0.313	0.360	1.000	1.152	1.152	1.152	-0.998
b series D05	1:10	1:2	0.319	0.319	0.344	1.000	1.078	1.078	1.078	-1.000
	1:10	1:4	0.315	0.315	0.354	1.000	1.124	1.124	1.124	-1.000
	1:10	1:8	0.313	0.313	0.360	1.000	1.152	1.152	1.152	-1.000
c series, D2	1:10	1:2	0.320	0.319	0.344	0.997	1.076	1.078	1.076	-0.932
	1:10	1:4	0.316	0.315	0.354	0.995	1.118	1.124	1.118	-0.915
	1:10	1:8	0.315	0.312	0.359	0.990	1.139	1.151	1.139	-0.862
c series, D1	1:10	1:2	0.319	0.319	0.344	1.000	1.078	1.078	1.078	-0.992
	1:10	1:4	0.315	0.315	0.354	0.999	1.123	1.124	1.123	-0.989
	1:10	1:8	0.313	0.313	0.360	0.999	1.150	1.152	1.150	-0.983
c series D05	1:10	1:2	0.319	0.319	0.344	1.000	1.078	1.078	1.078	-0.999
	1:10	1:4	0.315	0.315	0.354	1.000	1.124	1.124	1.124	-0.999
	1:10	1:8	0.313	0.313	0.360	1.000	1.152	1.152	1.152	-0.998
d series, D2	1:10	1:2	0.320	0.319	0.344	0.998	1.075	1.078	1.075	-0.941
	1:10	1:4	0.316	0.315	0.353	0.996	1.118	1.123	1.118	-0.927
	1:10	1:8	0.315	0.312	0.359	0.991	1.139	1.149	1.139	-0.880
d series, D1	1:10	1:2	0.319	0.319	0.344	1.000	1.078	1.078	1.078	-0.993
	1:10	1:4	0.315	0.315	0.354	0.999	1.123	1.124	1.123	-0.991
	1:10	1:8	0.313	0.313	0.360	0.999	1.150	1.151	1.150	-0.985
d series D05	1:10	1:2	0.319	0.319	0.344	1.000	1.078	1.078	1.078	-0.999
	1:10	1:4	0.315	0.315	0.354	1.000	1.124	1.124	1.124	-0.999
	1:10	1:8	0.313	0.313	0.360	1.000	1.152	1.152	1.152	-0.998
e series, D2	1:10	1:2	0.320	0.320	0.344	1.000	1.076	1.076	1.076	-1.000
	1:10	1:4	0.316	0.316	0.353	1.000	1.118	1.118	1.118	-1.000
	1:10	1:8	0.314	0.314	0.358	1.000	1.139	1.139	1.139	-1.000
e series, D1	1:10	1:2	0.319	0.319	0.344	1.000	1.078	1.078	1.078	-1.000
	1:10	1:4	0.315	0.315	0.354	1.000	1.123	1.123	1.123	-1.000
	1:10	1:8	0.313	0.313	0.360	1.000	1.150	1.150	1.150	-1.000
e series D05	1:10	1:2	0.319	0.319	0.344	1.000	1.078	1.078	1.078	-1.000
	1:10	1:4	0.315	0.315	0.354	1.000	1.124	1.124	1.124	-1.000
	1:10	1:8	0.313	0.313	0.360	1.000	1.152	1.152	1.152	-1.000
f series, D2	1:10	1:2	0.320	0.320	0.343	1.000	1.075	1.075	1.075	-1.000
	1:10	1:4	0.316	0.316	0.353	1.000	1.116	1.116	1.116	-1.000
	1:10	1:8	0.314	0.314	0.357	1.000	1.135	1.135	1.135	-1.000
f series, D1	1:10	1:2	0.319	0.319	0.344	1.000	1.078	1.078	1.078	-1.000
	1:10	1:4	0.315	0.315	0.354	1.000	1.123	1.123	1.123	-1.000
	1:10	1:8	0.313	0.313	0.360	1.000	1.150	1.150	1.150	-1.000
f series D05	1:10	1:2	0.319	0.319	0.344	1.000	1.078	1.078	1.078	-1.000
	1:10	1:4	0.315	0.315	0.354	1.000	1.124	1.124	1.124	-1.000
	1:10	1:8	0.313	0.313	0.360	1.000	1.152	1.152	1.152	-1.000

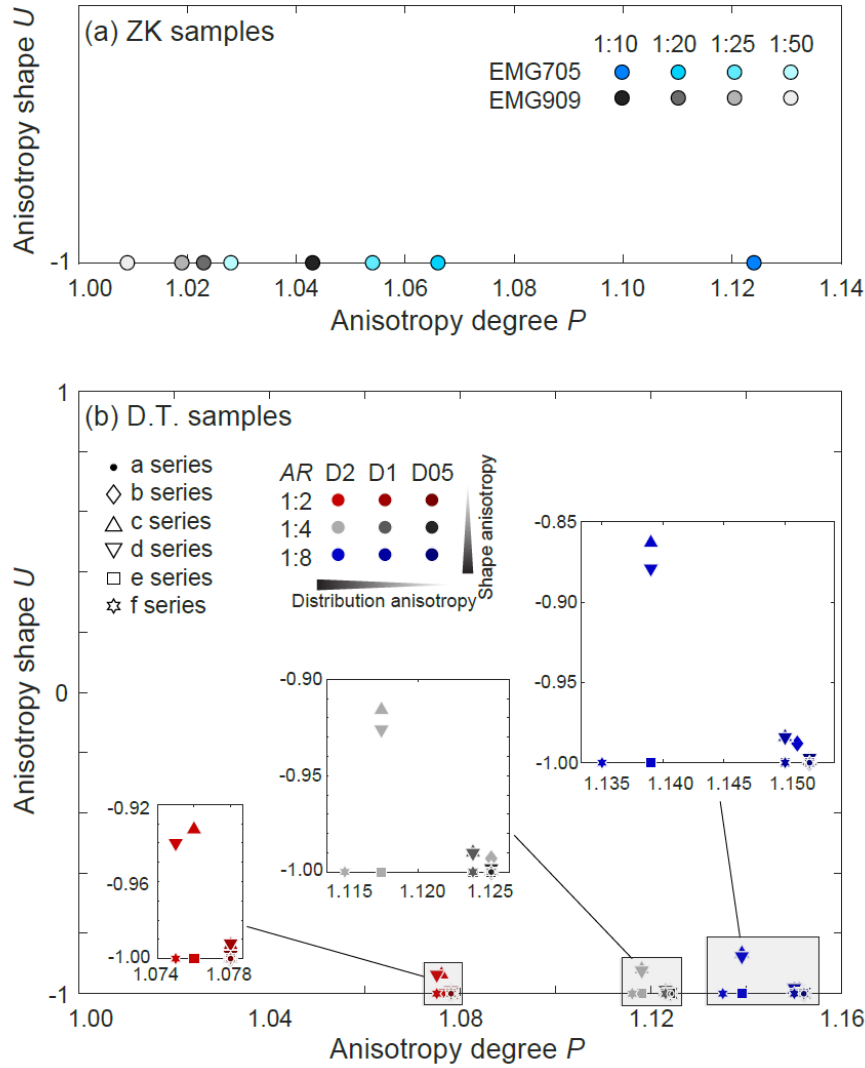


Fig. 4: Model results for (a) ZK sample series, with constant aspect ratio of the void and variable fluid concentration, and (b) D.T. sample series, using water-based fluid at 1:10 concentration, three aspect ratios (AR, diameter:height) of each void, and a series of filled void distributions.

### 2.3.1 ZK sample series

AC susceptibility was measured in several fields, frequencies, and along two or three axes of the sample coordinate system ( $k_x$ ,  $k_y$  and  $k_z$ , or  $k_x$  and  $k_z$ ; where the z-axis is along the cylinder axis, and the x- and y-axes oriented arbitrarily in the plane perpendicular to that axis). In combination with constraints from the known sample geometry (rotational symmetry around z), two directions are sufficient to determine the magnetic anisotropy tensor, and three directions allow to estimate data quality. Additional estimates of data quality were obtained from repeat measurements.



Two instruments were initially used for directional susceptibility measurements, (1) the MFK1-FA susceptibility bridge with three frequencies (976 Hz, 3904 Hz and 15616 Hz), and field ranges 2-706 A/m at 976 Hz, 2-356 A/m at 3904 Hz and 2-218 A/m at 15616 Hz; and (2) the SM150H/L susceptometers with nominal frequency range 63 Hz – 512 kHz. Of these, a reduced range between 500 Hz – 512 kHz provided usable results, whereas lower frequencies were subject to large noise levels. Measurements on the SM150H/L were conducted in 80 A/m, the highest field available at all frequencies. For anisotropy determination on the MFK1-FA, a field of 200 A/m was used and 3-5 repeat measurements were taken for each direction, while field-dependence measurements contain one measurement per field, and the measurement uncertainty is calculated from the measurements at the previous and subsequent fields. On the SM150H/L susceptometers, a total of 20 repeat measurements were necessary due to the larger instrumental noise level.

The magnetization of a sample exposed to an AC field can vary in-phase with the field, or be subject to a phase shift. This phase shift may arise from viscous relaxation in small particles, electrical eddy currents in conductive materials or weak-field hysteresis (Jackson, 2003-2004, Hrouda *et al.*, 2017). While the SM150H/L system measures the component of susceptibility in-phase with the field, the MFK1-FA also provides information on the phase shift. However, note that unlike on the KLY5 kappabridge, the zero phase is not calibrated on the MFK1 kappabridges. Here, the phase measured for the samples was corrected with the phase measured on the calibration sample with known zero phase, according to the method outlined in Hrouda *et al.* (2015).

The diamagnetic susceptibility of the holder and polycarbonate sample cylinder were subtracted from all measurements as background. After background-correction, the measured susceptibility was normalized by (1) sample volume and (2) void volume. The directional susceptibilities and the anisotropy of susceptibility, as described by the ratios of directional susceptibilities as well as  $P$  and  $U$  values were then compared to the expected values.

### 2.3.2 D.T. sample series

Based on the results obtained from the ZK samples, a subset of the above measurements was selected for the D.T. sample series. All measurements were performed on the MFK1-FA, and directional susceptibilities ( $k_x$ ,  $k_y$ ,  $k_z$ ) were measured at a field of 200 A/m, and frequencies of 976 Hz, 3904 Hz and 15616 Hz. Three to five repeat measurements were used to estimate directional susceptibilities and the measurement noise. Prior to filling the voids successively with ferrofluid, the empty cubes were measured under the same conditions, and later subtracted as background. The results are reported as directional susceptibilities normalized by sample or void volume, susceptibility ratios, or the anisotropy parameters  $P$  and  $U$  as for the ZK samples.

## 3. Results

### 3.1 ZK samples

#### 3.1.1 First set of ZK samples: Frequency and field dependence, instrumental noise

The susceptibility of samples filled with water- and oil-based ferrofluid is frequency-dependent, and the decrease in susceptibility with increasing frequency is stronger in the water-based ferrofluid compared to the oil-based ferrofluid (Fig. 5a; Table A, Supplementary Material). For the measurements obtained on the SM150H/L instruments, the susceptibility at 512 kHz is 35% - 43% of that at 500 Hz for ZK1 and ZK2 filled with water-based fluid. Conversely, the susceptibility of the oil-based fluid decreases less, to 74-77 % of the value at 500 Hz. The corresponding measurements of ZK3 and ZK4 are not interpretable due to the large instrumental noise level. The ratio of susceptibility at 16 kHz to that at 1 kHz ( $k_{16}/k_1$ ) as measured on the SM150H/L varies between 64% and 69% (water-based ferrofluid), and between 92% and 95% (oil-based fluid) for ZK1 and ZK2. The lower noise level of the MKF1 susceptibility bridge allows to analyse all samples, and the ratios  $k_{16}/k_1$  are 65%-66% for the majority of measurements for the water-based ferrofluid, and 85% - 102% for the oil-based ferrofluid. Compared to the initial susceptibilities from the fluids' technical specifications, the median effective susceptibilities at ~1kHz and ~16kHz are ~31% ( $k_1/k_i$ ) and ~21% ( $k_{16}/k_i$ ) for the water-based fluid EMG705, while they are approximately 130% and 120% for the oil-

based fluid EMG909. These ratios were calculated by comparing the measured directional susceptibilities to the expected directional susceptibilities reported in Table 1. Note that the ratios  $k_1/k_i$  and  $k_{16}/k_i$  are subject to large variability and also time-dependence; e.g., the effective susceptibility of oil-based fluid at 1:50 is approximately 3 times the expected value, likely related to the increased magnetic interactions when particles are aggregated.

The measurements obtained on both instruments agree within measurement uncertainty (Fig. 5b). The lower susceptibility of ZK1 filled with water-based fluid as measured on the MFK1-FA compared to the SM150H/L is related to loss of fluid from the cavity due to capillary motion of the fluid under the seal (cf Fig. 3). The noise level of the SM150H/L is several orders of magnitude larger than that of the MFK1-FA, and reaches >100% of the measured susceptibility. In comparison, variability for repeat measurements on the MFK1-FA is maximum 1-5% of the measured susceptibility (Fig. 5c). Therefore, although the SM150H/L is preferable in that it covers a larger frequency range, the quality of the data is not sufficient to analyse the anisotropy of the samples studied here, with expected  $P$ -values of 1.05 (water-based ferrofluid at 1:25) or 1.02 (oil-based fluid at 1:25).

Phase shifts are observed for both the oil-based and water-based ferrofluids (Fig. 5d). For both types of fluid, the phase is generally larger at ~4 kHz compared to 1 or 16 kHz. Samples filled with water-based fluid show higher phase shifts (up to ~16°) and more variability than those filled with oil-based fluid, where the maximum phase is ~8°.

Field-dependence measurements show that susceptibility and to a lesser degree phase are independent of applied field (Fig. 6). Some jumps are observed in the field-dependent data, but these are caused by changes in the dynamic range of the instrument and not sample properties.

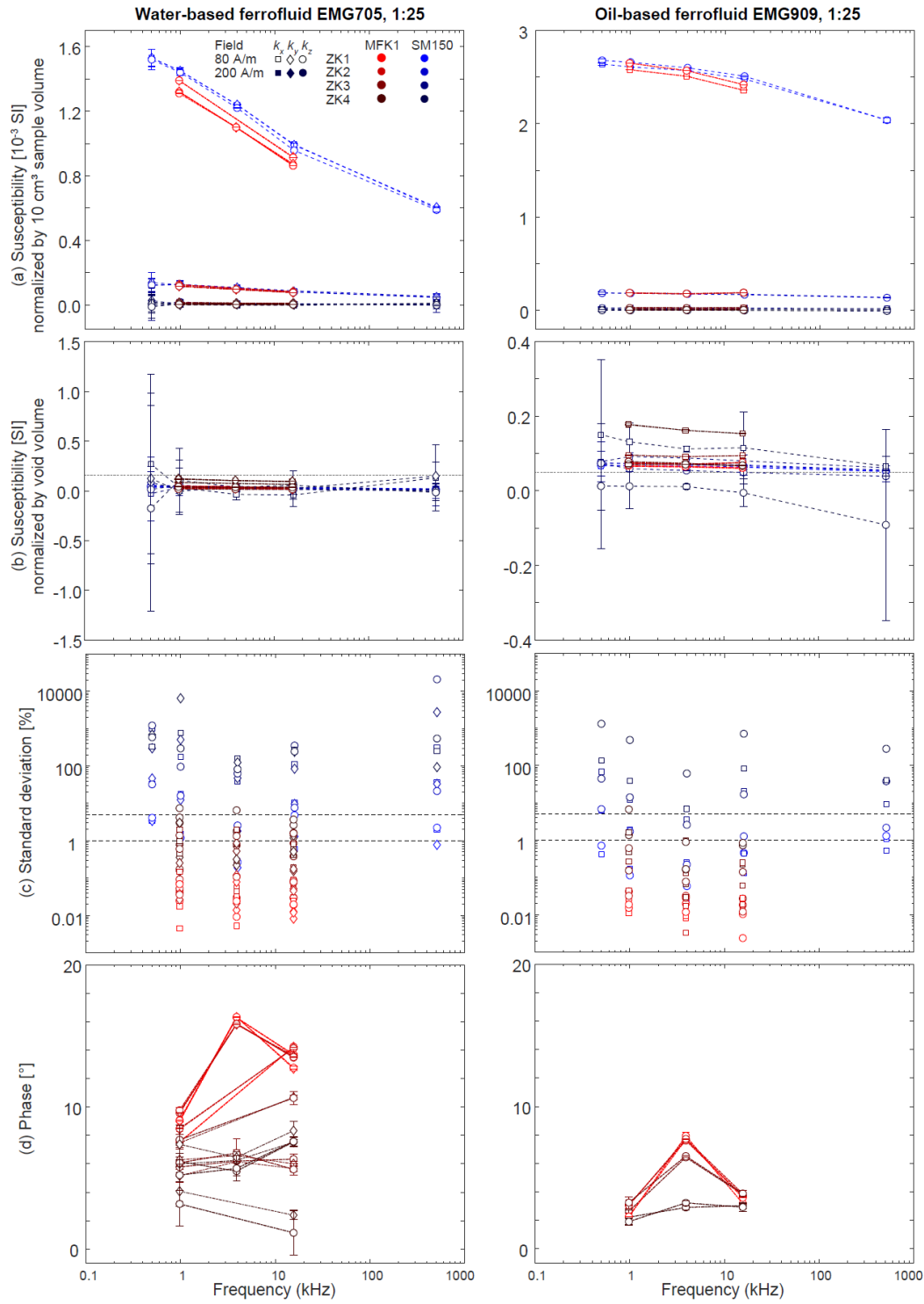


Fig. 5: Frequency dependence of susceptibility and phase shift for the ZK samples: Frequency-dependence of susceptibility normalized by sample (a) and void volume (b). Measurement frequencies for the MFK1-FA are  $\sim 1$  kHz,  $\sim 4$  kHz and  $\sim 16$  kHz, and for the SM150H/L, measurements were performed at 0.5 kHz, 1 kHz, 4 kHz, 16 kHz, and 512 kHz. (c) Measurement uncertainty given as percentage of standard deviation and mean of repeated measurements. Dashed lines indicate a 'standard' 1% noise level desirable for anisotropy measurements, and 5% noise, reflecting the expected anisotropy of the water-based fluid filled ZK samples. (d) Phase shift of the susceptibility.

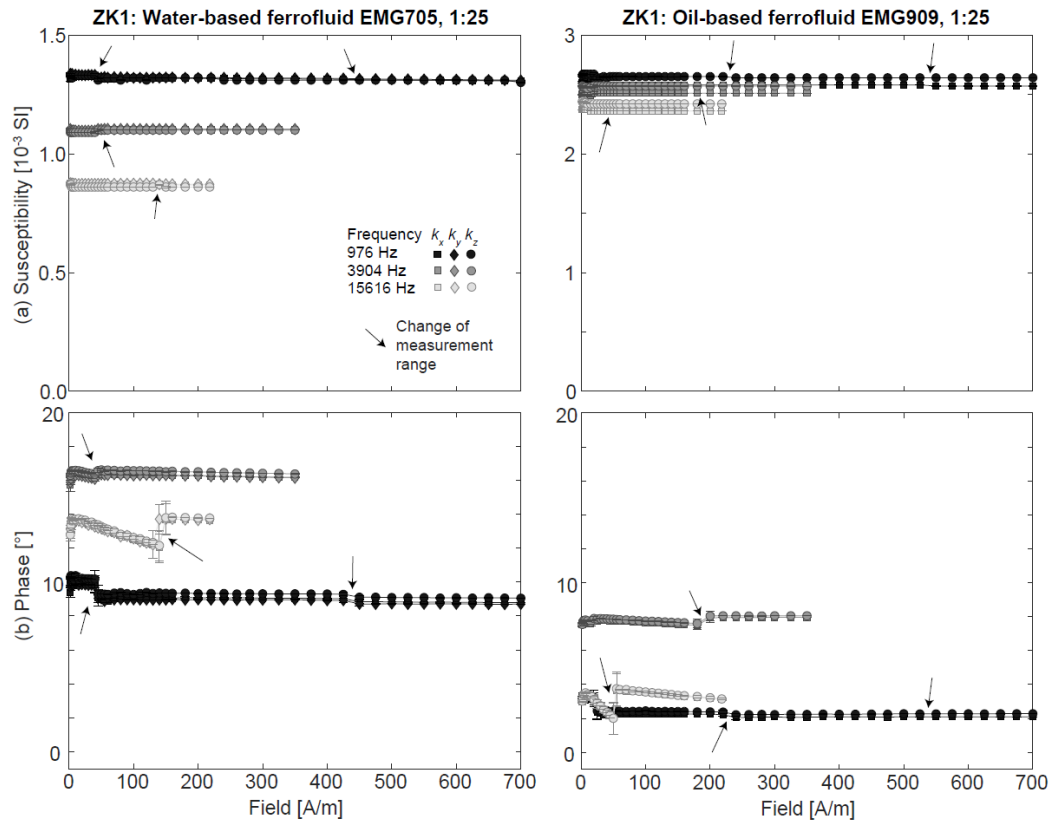


Fig. 6: Field dependence of susceptibility (a) and phase shift (b) for the ZK1 samples at frequencies  $\sim 1$ ,  $\sim 4$  and  $\sim 16$  kHz. Note that the jumps in susceptibility and associated larger errors are related to changes in the dynamic range of the instrument during the measurement (indicated by arrows).

Note that although the maximum susceptibility is expected along the sample z-axis, with  $k_x = k_y$ , this is not consistently observed in this initial dataset. The most likely explanation are the artefacts shown in Fig. 3, particularly fluid trapped at the interface between sample cylinder and seal, or fluid mixed with glue, and to a lesser degree trapped air inside the void. Although volumetrically small, the fluid trapped between the sample and seal appears to dominate the observed anisotropy in some samples. Anisotropy was therefore studied on the second set of samples, taking special care to avoid artefacts as much as possible during preparation.

### 3.1.2 Second set of ZK samples: Anisotropy and its dependence on concentration and frequency

Based on the initial results, a reduced number of measurements was conducted on the second set of samples. At the same time, additional aspects were investigated, e.g., the influence of ferrofluid

concentration, and time-dependence. Although preparation artefacts could not be prevented entirely, they were less prominent than in the first set of samples, allowing the analysis of the anisotropy of the ferrofluid-filled voids. Anisotropy depends both on the ferrofluid type, concentration and the measurement frequency. Additionally, measured anisotropy changes over time, reflecting the formation of air bubbles or particle aggregation.

Samples filled with water-based ferrofluid generally show the expected behaviour of  $k_z > k_x$ ,  $k_x \sim k_y$  (Fig 7a,b; Table A, Supplementary Material). Only the samples with the smallest voids, ZK4, display a behaviour contrary to expectation, in that their maximum susceptibility is often not parallel to the long axis of the cylinder. A possible explanation is that these small voids are the hardest to fill, and any fluid outside the void, or air bubbles trapped inside the void may outweigh the anisotropy of the fluid in the void itself. ZK4 results will thus not be interpreted further. For ZK1, ZK2 and to a lesser extent ZK3, a trend of stronger anisotropy degree (approximated here by  $k_z/k_x$ ) for higher concentration of ferrofluid is observed; however, the  $k_z/k_x$  ratios are lower than predicted in Table 1. Most samples show similar properties for the initial and repeat measurements after 25 days, but sometimes the degree of anisotropy decreased over time. This is interpreted here as the partial loss of fluid from the void, and its migration to the interface between plastic cylinder and glue. The anisotropy shapes are mostly prolate, as expected from the sample geometry (Fig. 7c).

MPFs of samples filled with oil-based fluid show large variability, and different behaviours for 1:50 concentration compared to 1:10 or 1:20. At concentrations of 1:10 or 1:20, the measured  $k_z/k_x$  ratios cluster loosely around the expected values, except for the repeat measurements after 25 days, which have significantly larger  $k_z/k_x$  ratios. Conversely, oil-based fluid concentrations of 1:50 lead to  $k_z/k_x$  mostly  $< 1$ , opposite of the expected behaviour, and the ratios decreased further after 25 days (Fig. 7a). This observation can be explained by the aggregation and precipitation of particles that is strongest at the 1:50 concentration, leading ultimately to an oblate body of precipitated particles at the bottom of the prolate void. Particle aggregation and precipitation is also accompanied by a

change of the anisotropy shape, from mostly prolate (as expected) at 1:10 or 1:20 concentration, to oblate at a concentration of 1:50 (Fig. 7c). The MPFs of the samples filled with 1:50 oil-based ferrofluid are clearly dominated by artefacts resulting from particle precipitation and are not related to the sample geometry. Hence, they are not discussed further.

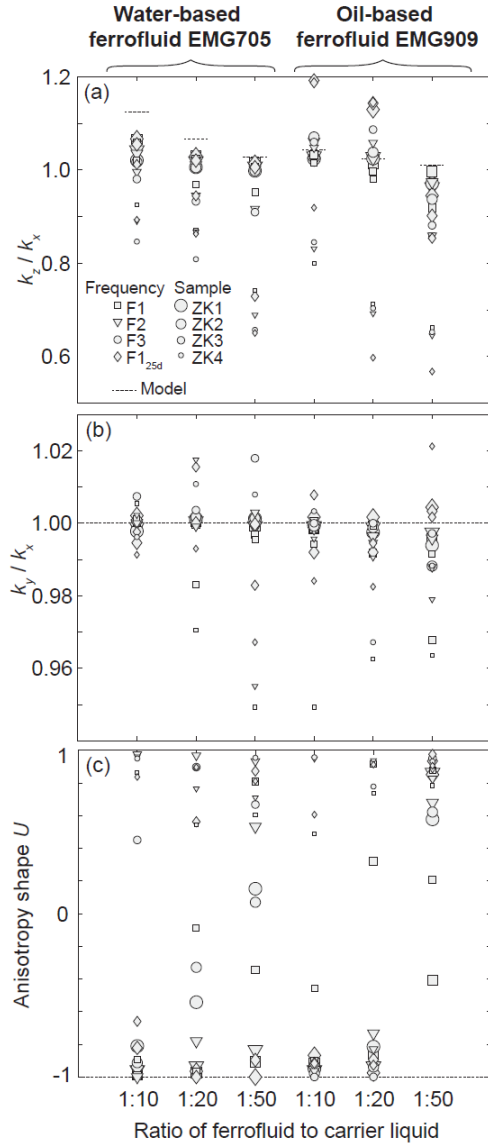


Fig. 7: Magnetic anisotropy of ferrofluid-filled voids in the second set of ZK samples, measured at 976 Hz (F1), 3904 Hz (F2), and 15616 Hz (F3). (a) Ratio of directional susceptibilities  $k_z$  to  $k_x$ , compared to the expected value from the model shown in Fig. 4a. (b) Ratio of directional susceptibilities  $k_y$  to  $k_x$ . Due to sample symmetry, susceptibilities should be equal along these two directions, indicated by the dashed line. (c) Anisotropy shape  $U$ , which should be -1 (dashed line) according to sample symmetry. Measurements at F1 were repeated after the sample had been stored for 25 days, and symbol sizes reflect the size of the void in the ZK1, ... ZK4 samples.

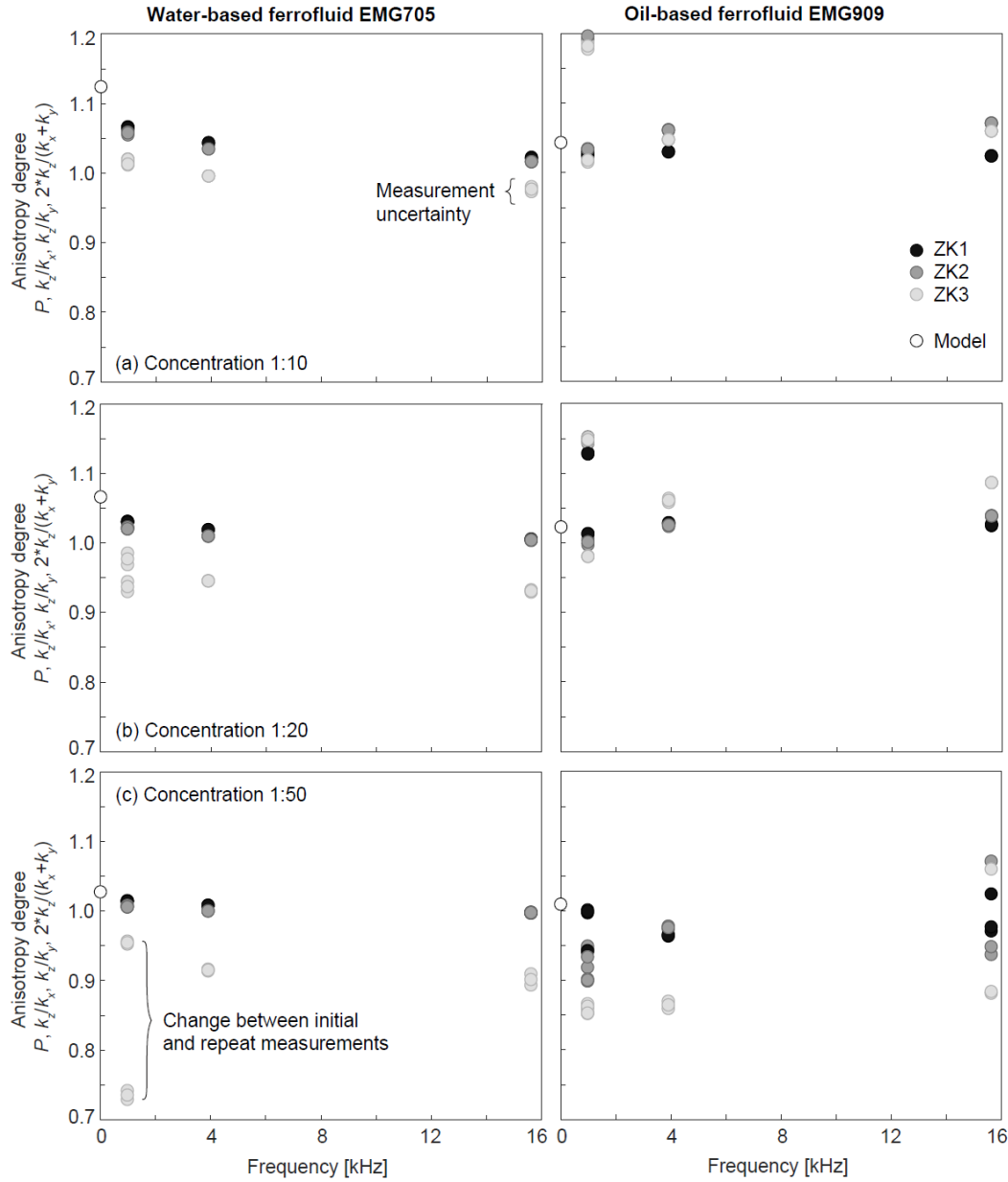


Fig. 8: Comparison of the measured ratios  $k_z/k_x$ ,  $k_z/k_y$  and  $2*k_z/(k_x+k_y)$  with the modelled  $P$ -value in the frequency range  $\sim 1$  kHz to  $\sim 16$  kHz, for different ferrofluid concentrations, 1:10 (a), 1:20 (b), and 1:50 (c). Due to the symmetry in the  $x$ - $y$ -plane, all these measured parameters are approximations of the modelled anisotropy degree, they should be equal and their variability indicates deviation from ideal behaviour. Large variability is observed in oil-based samples due to artefacts such as particle aggregation and poor sealing.

Higher measurement frequencies almost always result in weaker anisotropy degrees for samples filled with water-based EMG705 (Figs 7a and 8). This observation can be directly related to the decrease in mean susceptibility with increasing frequency (cf Fig. 5). The frequency-dependence of



the MPF anisotropy degree is less clear for samples filled with oil-based EMG909. A possible explanation for this is that the effective susceptibility shows overall a smaller frequency-dependence for the oil-based fluid. A second possibility is that the time-dependent artefacts (particle aggregation, chemical reaction between oil-based ferrofluid and glue destroying the seal) dominantly control the magnetic results of these samples.

### 3.2 D.T. samples

The anisotropy results of the D.T. samples show the combined effects of shape and distribution anisotropies for different aspect ratios of the voids, and as successively more voids are filled with EMG705 water-based ferrofluid (Fig. 9; Table B, Supplementary Material). The measured anisotropy shapes are mainly prolate, similar to expectation, except for the samples with the smallest voids (0.5 mm diameter), and measurements at 15616 Hz (F3) in the a, b, and c series. The reason the D05 samples display MPF shapes different from the expected sample geometry or results of the D1 and D2 samples containing larger voids, are preparation artefacts (cf Fig 3). Similar to the ZK4 samples, the voids in the D05 samples are not filled completely with ferrofluid, making the spatial variation of susceptibility and magnetization more complex than the sample geometry. The deviation in shape for the a, b, and c series measured at F3 are likely related to these measurements having the largest noise level. The susceptibility and its anisotropy are expected to be lowest at F3, and the smaller the number of filled voids, the smaller the expected susceptibility. Measured shapes for corresponding samples in the D1 and D2 series are almost identical. For a given measurement frequency and configuration of filled voids, the degree of anisotropy increases with the aspect ratio of the individual voids. The measured degree of anisotropy is almost always smaller than that expected, and generally decreases nonlinearly with increasing measurement frequency (Fig. 10).

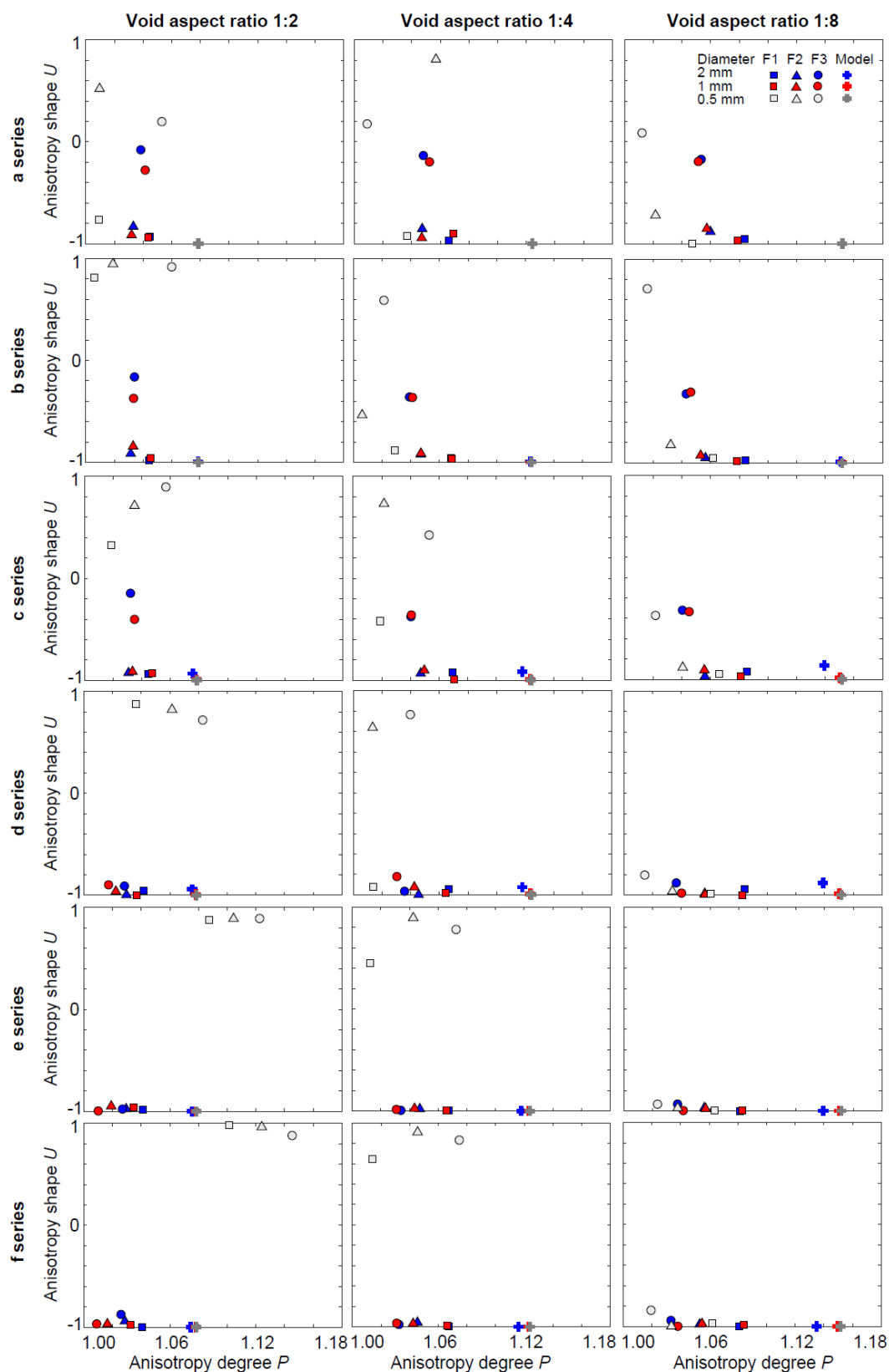


Fig. 9: Modelled and measured anisotropy degree  $P$  and shape  $U$  for the D.T. samples, filled with water-based EMG705 fluid at concentration 1:10. Measurements were performed at 3 frequencies, 976 Hz (F1), 3904 Hz (F2), and 15616 Hz (F3). Preparation artefacts are observable in the D05 sample series.

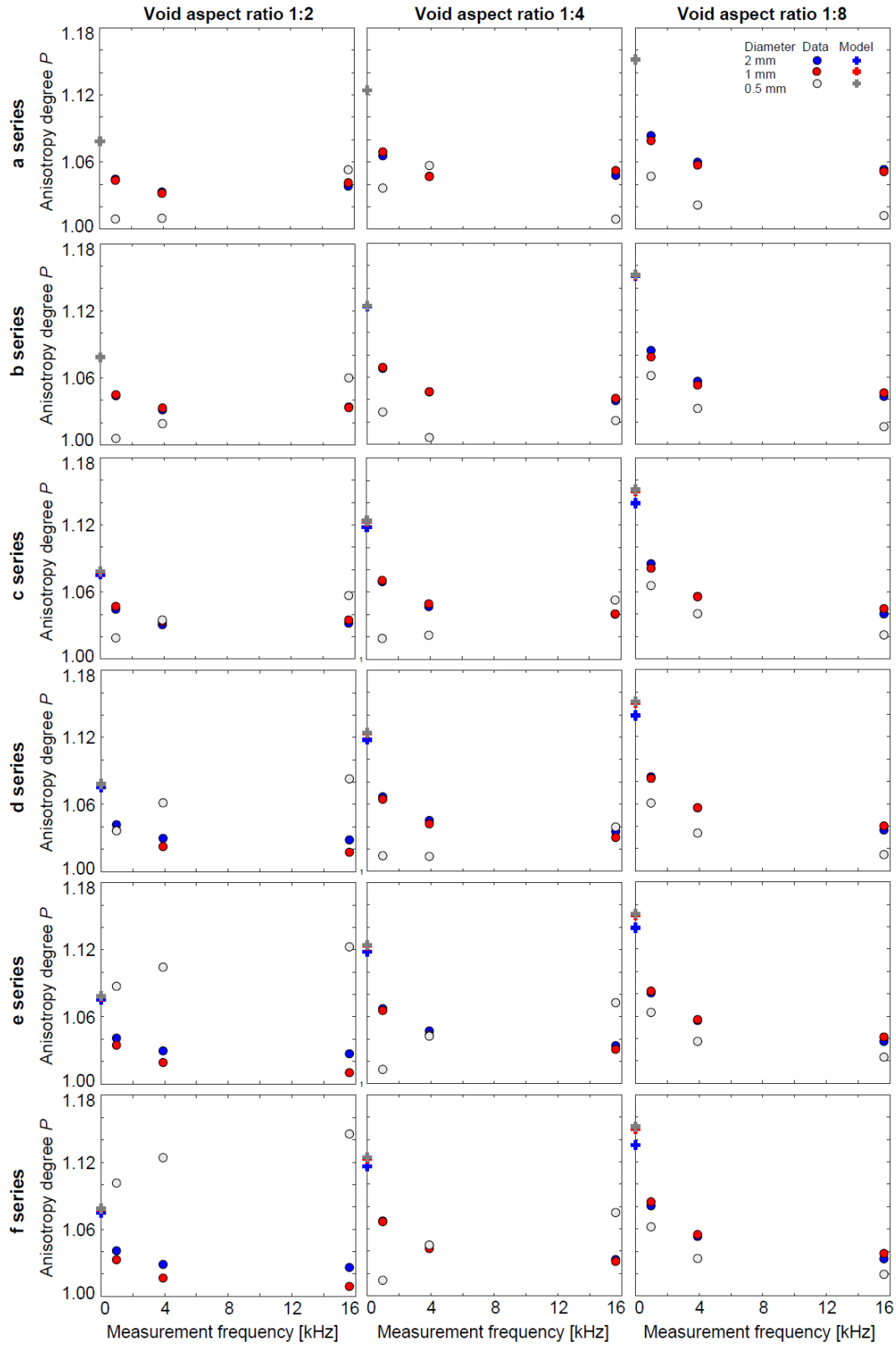


Fig. 10: Frequency dependence of the anisotropy degree  $P$  for the D.T. samples filled with EMG705 water-based ferrofluid at 1:10 concentration. Measurements were performed at the standard frequencies of the MFK1-FA kappabridge, 976 Hz, 3904 Hz, and 15616 Hz. Preparation artefacts are visible in the D05 series. The results for the D1 and D2 samples indicate a decrease of anisotropy degree with increasing measurement frequency.

## 4. Discussion

### 4.1 Frequency-dependence leads to discrepancies between expected and measured anisotropy

A major finding of this study is the strong frequency-dependence of the magnetic susceptibility of the ferrofluid and its anisotropy, in particular for the water-based EMG705. This frequency-dependence leads to large discrepancies between the initial susceptibilities reported in the fluid's technical specifications, valid for measurements in weak DC fields, and the effective properties at standard measurement conditions for MPF studies. Self-demagnetization and hence shape anisotropy increase nonlinearly with the intrinsic fluid susceptibility. Observed deviations between expected and measured anisotropy degrees in samples filled with EMG705 are clearly related to the effective fluid susceptibility being lower than the specified initial susceptibility. Analogously, the measured anisotropy degree of samples filled with EMG909 should be slightly higher than that modelled, due to the higher effective susceptibility. However, this deviation is low compared to the variability in the data, so that no unambiguous conclusion can be drawn. Measurements of the EMG909-filled samples after 25 days show stronger anisotropies, possibly associated with an increase in fluid susceptibility resulting from particle aggregation. In general, the measured MPF of a given sample will depend on the measurement frequency in addition to ferrofluid type and concentration, and all of these parameters (or the effective fluid susceptibility at measurement conditions) need to be known before MPFs can be interpreted quantitatively. The intrinsic susceptibility at measurement conditions can be determined by measuring directional susceptibilities of fluid in a void of known shape and dimensions under the same conditions, and then calculating  $k_{int} = (I + k_{obs}N)^{-1}k_{obs}$  (e.g. Clark, 2014). Note that  $k_{obs}$  approaches  $N^{-1}$  for large  $k_{int}$ , so that high intrinsic susceptibilities cannot be measured reliably. In this case it may be helpful to measure diluted fluid and then calculate  $k_{int}$  of the undiluted fluid from  $k_{int}$  of the diluted fluid and the dilution ratio. In any case, we recommend to do several repeat measurements of  $k_{obs}$ , as any uncertainty will be amplified when calculating  $k_{int}$ , especially when  $N$  is large along the measurement direction.

513 Only one MPF study so far specified the measurement frequency used, which was 976 Hz (Parés *et*  
514 *al.*, 2016). In some additional studies, the frequencies can be estimated from the instrument  
515 capabilities, and range from 750 Hz to 920 Hz (Pfleiderer and Halls, 1990, Pfleiderer and Halls, 1993,  
516 Pfleiderer and Halls, 1994, Hrouda *et al.*, 2000, Benson *et al.*, 2003, Jones *et al.*, 2006, Esteban *et al.*,  
517 2006, Robion *et al.*, 2014, Humbert *et al.*, 2012). Where neither the instrument nor measurement  
518 frequency are specified (Pfleiderer and Kissel, 1994, Louis *et al.*, 2005, Almqvist *et al.*, 2011), or  
519 where instruments with several operating frequencies were used (Nabawy *et al.*, 2009), anisotropy  
520 degrees are not interpretable, and derived empirical relationships not comparable to other studies.

521 Measurement frequencies just below 1 kHz appear most common in MPF studies, and it would be  
522 desirable to define a universal relationship between the initial susceptibility of a ferrofluid and its  
523 effective susceptibility at  $\sim 1$  kHz. This would allow correction of previously published results and  
524 empirical relationships for differences between the initial and effective fluid susceptibilities, and  
525 facilitate modelling in future studies. However, the two ferrofluids used here, EMG705 and EMG909,  
526 show largely different characteristics: for EMG705, the effective susceptibility at  $\sim 1$  kHz is  $\sim 20$ - $35\%$   
527 of its initial susceptibility, and for EMG909 the ratio of effective to initial susceptibility is  $\sim 125$ - $150\%$ .

528 A consequence of this is that although the technical specifications (ferrotec.com) indicate a larger  
529 susceptibility for EMG705 than EMG909, the effective susceptibilities at 976 Hz, 3904 Hz and 15616  
530 Hz are higher for EMG909. Hence, the frequency-dependence and ratio of effective to initial  
531 susceptibilities need to be measured for each ferrofluid used in MPF studies.

532 Some previous MPF studies used the same fluids that are investigated here, EMG705 (Pfleiderer and  
533 Halls, 1990, Pfleiderer and Halls, 1993, Pfleiderer and Halls, 1994, Pfleiderer and Kissel, 1994), and  
534 EMG909 (Robion *et al.*, 2014, Parés *et al.*, 2016). Other fluids used include EMG905 (Hrouda *et al.*,  
535 2000, Benson *et al.*, 2003, Jones *et al.*, 2006, Almqvist *et al.*, 2011), EMG507 (Robion *et al.*, 2014),  
536 and EMG509 (Humbert *et al.*, 2012), and the type of ferrofluid was not always specified (Hailwood *et*  
537 *al.*, 1999, Louis *et al.*, 2005, Esteban *et al.*, 2006, Nabawy *et al.*, 2009). It is possible that all water-

based fluids show a similar frequency-dependence as EMG705, and all oil-based fluids a behaviour similar to EMG909. If this is the case, it would explain why the empirical correlations between the MPF anisotropy degree and pore aspect ratios are steeper in the study of Jones *et al.* (2006) compared to (Pfleiderer and Halls (1990, 1993); it could be an effect of the higher effective fluid susceptibilities in the former study compared to the later. The correlations with respect to permeability are not comparable because essential information on the fluid properties and measurement frequencies are missing. More work will be needed to determine the effective properties of all ferrofluids used in MPF studies, and to systematically compare empirical relationships.

## 4.2 Origin of the frequency-dependence

The measurements show frequency-dependent susceptibility and a phase shift, but no significant field-dependence (cf. Figs 5 and 6). Both frequency-dependence and phase shift are larger for samples filled with EMG705 water-based fluid compared to the EMG909 oil-based fluid. Three mechanisms have been described to cause frequency-dependence and out-of-phase susceptibility: (1) viscous relaxation of superparamagnetic particles, (2) eddy currents in conductive materials, and (3) weak-field hysteresis (Jackson, 2003-2004, Hrouda *et al.*, 2013, Jackson *et al.*, 1998, Néel, 1949, Brown, 1959, Dormann, 1981). The absence of any field-dependence (cf Fig. 6) makes it possible to exclude weak-field hysteresis as a phenomenon occurring in the samples investigated here (Hrouda *et al.*, 2013). The electrical conductivities of both ferrofluids at concentration 1:25 were measured at the Petrophysics Laboratory at the University of Bern; EMG705 has an electrical conductivity of 2 mS while that of EMG909 is not measurable, so that eddy currents likely do not contribute to dissipation in these samples. Therefore, the observed frequency-dependence and out-of-phase susceptibilities are a result of viscous relaxation, either by Néel relaxation or Brownian motion.

Both Néel and Brownian relaxation times vary with particle volume. The Néel relaxation time  $\tau_N$  is computed as  $\tau_N = \tau_0 \exp(KV/kT)$ , where  $\tau_0$  is a time constant,  $K$  the anisotropy constant,  $V$  the

particle volume, and  $kT$  the thermal energy, being the product of Boltzman's constant and temperature (Néel, 1949). The time constant  $\tau_0$  is not truly constant as it depends on particle size, coercivity and temperature; and varies between  $0.4 \cdot 10^{-9}$  s to  $3.3 \cdot 10^{-9}$  s for magnetite particles with sizes decreasing from 15 nm to 5 nm. A value of  $1 \cdot 10^{-9}$  s agrees with experimental evidence (Worm, 1998). The volume of a particle with 10 nm diameter is  $5.24 \cdot 10^{-25}$  m<sup>3</sup>, measurements were done at room temperature (298 K), and the  $K_1$  anisotropy constant for magnetite is  $1.35 \cdot 10^4$  J/m<sup>3</sup> (Syono, 1965). For these parameters,  $\tau_N = 5.6 \cdot 10^{-9}$  s.

The Brownian relaxation time has been described as  $\tau_B = \left(\frac{\gamma K}{M}\right) * \sqrt{KV/kT\pi} * \exp\left(-\frac{KV}{kT}\right)^{-1}$ , where  $\gamma$  is the gyromagnetic constant,  $1.76085963 \cdot 10^{11}$  (sT)<sup>-1</sup>, and M the magnetisation (Jones and Srivastava, 1989). We use 480 kA/m, i.e., the saturation magnetization of magnetite. For the 10 nm particles in the fluid, this leads to  $\tau_B = 1.5 \cdot 10^{-9}$  s.

These calculations indicate the both relaxation times have the same order of magnitude, and the Brownian relaxation is slightly faster. At the same time, Jones and Srivastava (1989) state that for small particles (<10<sup>6</sup> atoms), Néel's model provides more physically reasonable results. They also found both relaxation times to be similar for particles with 30 nm diameter, which is different from the results obtained here. Söffge and Schmidbauer (1981) report typical relaxation times of  $\tau_B = 10^{-3}$  s and  $\tau_N = 10^{-9}$  s for a ferrofluid with magnetite particles of 10 nm diameter. These values agree with the calculation shown here for  $\tau_N$ , but not for  $\tau_B$ . A reason for the discrepancy could be that they calculated  $\tau_B = \frac{3\eta V}{kT}$ , where  $\eta$  is the fluid viscosity. For the fluids used here,  $\eta < 5 \cdot 10^{-3}$  Pa\*s for EMG705, and  $\eta = 3 \cdot 10^{-3}$  Pa\*s for EMG909, leading to  $\tau_B = 1.1 - 1.9 \cdot 10^{-6}$  s, which is closer to their results, but still does not agree. Using this value, Brownian relaxation is significantly slower than Néel relaxation, indicating that Néel relaxation likely dominates. However, the large variability between calculations and studies indicates that these relaxation times need to be interpreted with care. Note that both relaxation times depend on particle size, so that the particle aggregation that was observed in the ferrofluids over time will affect the results. Because particle aggregation

appears fastest in strongly diluted EMG909 ferrofluid, the strongest artefacts are expected there. The lower stability of oil-based ferrofluid over time was also observed by Robion (pers. comm.). To ensure a stable magnetic response over time, we would thus recommend using water-based ferrofluid, or ferrofluid at higher concentration, in magnetic pore fabric studies.

Worm and Jackson (1999) describe the frequency-dependence of susceptibility due to viscous relaxation:  $X = (\mu_0 V M_s^2) / (3kT(1 + (2\pi f)^2 \tau^2))$ , where  $f$  is the measurement frequency. Using  $\tau_N = 5.6 * 10^{-9} s$ ,  $V = 5.24 * 10^{-25} m^3$ , and  $M_s = 480 kA/m$  results in no observable frequency-dependence at frequencies between 1-16 kHz. This may be related to the uncertainty in the relaxation times, or indicate that the magnetic particle size is smaller than 10 nm. The observed difference in frequency-dependence of EMG705 and EMG909, despite them having the same nominal size of 10 nm, may indicate that their actual sizes differ from each other, with the effective size of the EMG705 particles being smaller, and therefore showing a stronger frequency-dependence than EMG909 and predicted for 10 nm particles.

#### 4.3 Implications for the interpretation of MPF and impregnation efficiency data

Empirical relationships for MPFs focus on fabric orientation and anisotropy degree. The anisotropy degree, and in particular the variation of the  $P$ -value (and analogously the  $L$ - and  $F$ -values) with intrinsic fluid susceptibility are discussed here. For a given fluid susceptibility, the MPF anisotropy degree increases nonlinearly with pore aspect ratio, and corresponding empirical relationships have been used to efficiently estimate the average pore shapes or their alignment (Hrouda *et al.*, 2000, Jones *et al.*, 2006). However, the measured  $P$ -value also increases nonlinearly with ferrofluid susceptibility for any given pore aspect ratio. The effective intrinsic susceptibility depends on the type and concentration of ferrofluid, as well as the measurement frequency. Thus, all published empirical relationships depend on the effective intrinsic susceptibility of the respective fluids, so that a comparison between studies is not straightforward. For example, the MPF anisotropy degrees for a given pore shape reported in Jones *et al.* (2006) tend to be higher than those of Pfeleiderer and Halls



(1990), which are in turn larger than those in Pfeleiderer and Halls (1993). A partial explanation for this is that Jones *et al.* (2006) used a fluid with initial susceptibility  $k_i = 1.09$ , whereas Pfeleiderer and Halls (1993) used a fluid with  $k_i = 0.8$  (the susceptibility of the fluid in Pfeleiderer and Halls (1990) is not specified). However, careful comparison between the literature data and models indicates that the data by Jones *et al.* (2006) more closely matches the model for  $k_{int} = 2$ , and that of Pfeleiderer and Halls (1993) resembles a model with  $k_{int} < 0.5$  (Fig. 11a,b). Thus, the comparison between measured and modelled  $P$ -values indicates that the effective  $k_{int}$  of the EMG705 fluid in Pfeleiderer and Halls (1993) is lower, while the effective  $k_{int}$  of the EMG905 ferrofluid in the study by Jones *et al.* (2006) is higher than the reported initial susceptibilities. A lower than expected value could be due to dilution of the fluid, but the higher effective value can only be explained by a higher effective intrinsic susceptibility, related to frequency-dependent susceptibility. The measured  $k_{int}$  at  $\sim 1$  kHz ranges from  $\sim 20$  -  $\sim 35\%$  of the expected value for EMG705 (using ZK1 and ZK2 measurements shown in Fig. 2), and  $\sim 125\%$  -  $\sim 150\%$  of the expected value for EMG909. Hence, the frequency-dependence of the ferrofluid susceptibility strongly affects the measured  $P$ -values, as well as the empirical relationships between pore shape and MPF anisotropy degree. The combined dependence of the measured anisotropy degree on the effective  $k_{int}$  and the pore shape is summarized in Fig. 11c. The influence of the measurement frequency is further illustrated in Fig. 11d, which shows that the expected  $P$ -value for a prolate ellipsoidal void filled with pure EMG705 is  $> 2.5$ . In contrast, at the typical  $\sim 1$  kHz measurement frequency, the  $P$ -value of the same void and fluid is only  $\sim 1.5$ . At higher frequencies, the  $P$ -values are even lower. The frequency-related decrease in  $P$  is comparable to lowering the ferrofluid concentration to 1:25. These models additionally illustrate that higher fluid concentrations and lower measurement frequencies make it possible to detect weak anisotropies that may be below the detection limit if strongly diluted ferrofluids or high measurement frequencies are used. The relevance of the ferrofluid concentration has been described previously (Jones *et al.*, 2006, Biedermann, 2019), and the results presented here clearly indicate that measurement frequency may be equally relevant for the interpretation of MPF data.

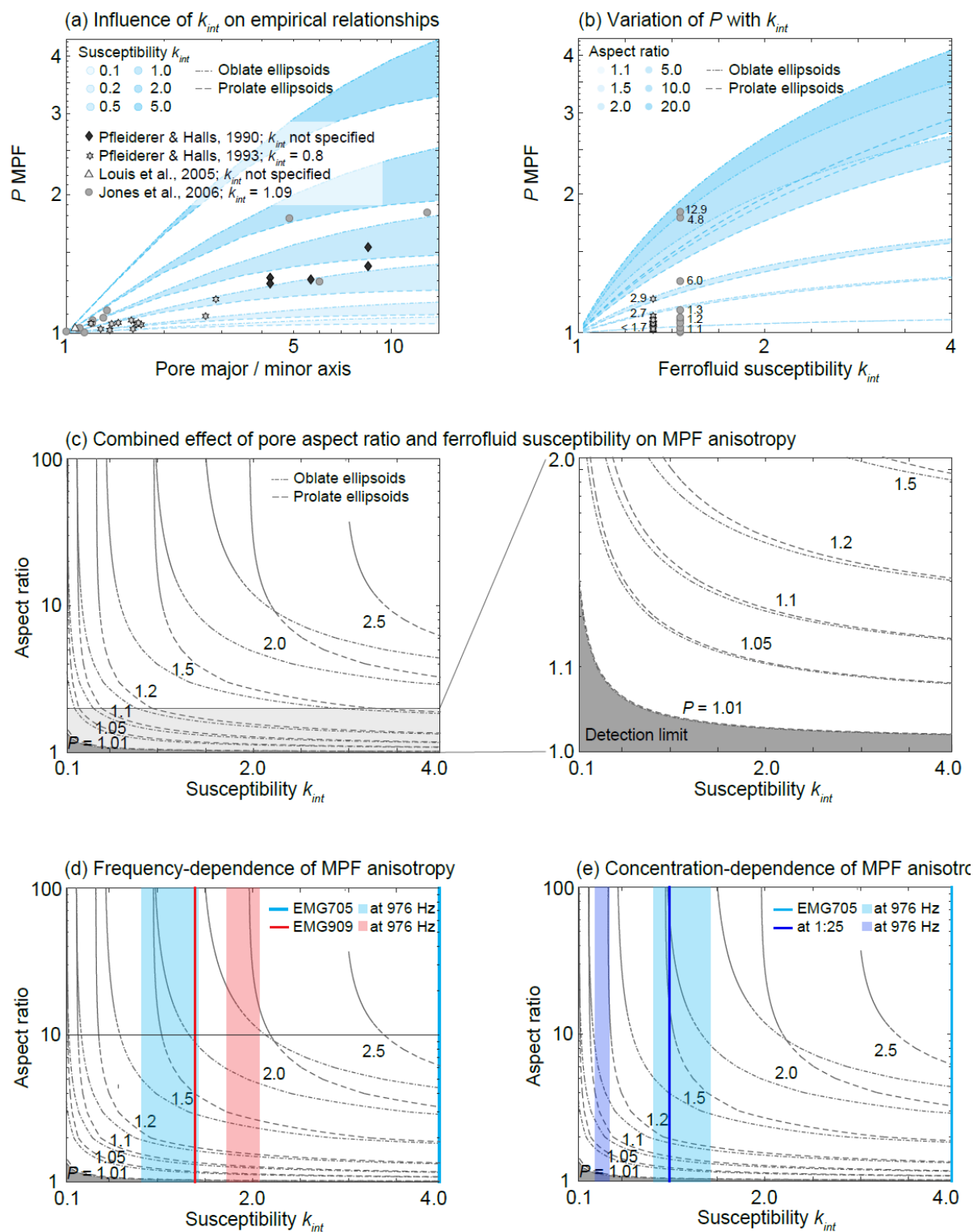


Fig. 11: (a) The influence of ferrofluid susceptibility on the MPF – pore shape relationships, where shaded areas reflect variability from rotationally oblate to rotationally prolate ellipsoidal pores with a given axial ratio. Published data are shown on top of the models. (b) Expected MPF  $P$ -values as function of fluid susceptibility. Data as in (a), but only datasets with known intrinsic susceptibility are shown. Numbers next to the data points reflect their axial ratios. (c) Variation of anisotropy degree as a function of pore axial ratio and ferrofluid intrinsic susceptibility combined, and effect of non-zero measurement frequency (d) or ferrofluid concentration (e).

647 Although the fabric orientation is not directly affected by the frequency-dependence of the  
648 ferrofluid susceptibility, the lower anisotropy degrees at higher frequencies may lead to lower signal  
649 to noise ratios. This in turn can result in higher uncertainty and larger confidence ellipses of the  
650 principal MPF directions. When noise levels are high, this results in unrealistically large  $P$ ,  $L$  and  $F$ -  
651 values, and also large uncertainties in anisotropy shape (Biedermann *et al.*, 2013), and this may  
652 explain some of the deviations from the generally observed trends in the D.T. a, b and c series for  
653 high frequencies. For most reliable estimations of pore fabrics, ferrofluids with high effective  
654 intrinsic susceptibilities at the measurement conditions are preferred. For EMG705 and possibly  
655 other water-based fluids, a frequency of  $\sim 1$  kHz is favourable compared to 4 kHz or 16 kHz. If an  
656 instrument with a comparable noise level at lower frequencies becomes available in the future, this  
657 may provide even better MPF results. For EMG909 and potentially other oil-based fluids, the  
658 frequency-dependence is less pronounced, so that measurements at different frequencies can be  
659 more easily compared. In both cases, highly concentrated ferrofluids are preferable in that they  
660 provide higher susceptibilities and stronger anisotropies that are easier to characterize.

661 Empirical relationships also exist between MPFs and permeability anisotropy. There, the  
662 interpretation is more challenging, as in addition to the considerations above, permeability depends  
663 on the volumetrically small connections between pores, while MPFs are dominantly defined by the  
664 shape and orientation of larger pores. Anisotropic permeability also controls the migration of fluid  
665 during impregnation, and may influence MPF results when impregnation efficiency is  $< 100\%$ .  
666 Further work is needed to fully characterize this effect.

667 In rock samples, impregnation efficiency, i.e., the percentage of the pore space that is filled with  
668 ferrofluid, is a crucial parameter that defines the quality and reliability of MPF-based interpretations.  
669 Impregnation efficiency has been determined using either the increase in mass, or the increase in  
670 susceptibility after impregnation compared to the dry sample, and by visual inspection on cut  
671 surfaces (Robion *et al.*, 2014, Parés *et al.*, 2016, Almqvist *et al.*, 2011). If impregnation efficiency is

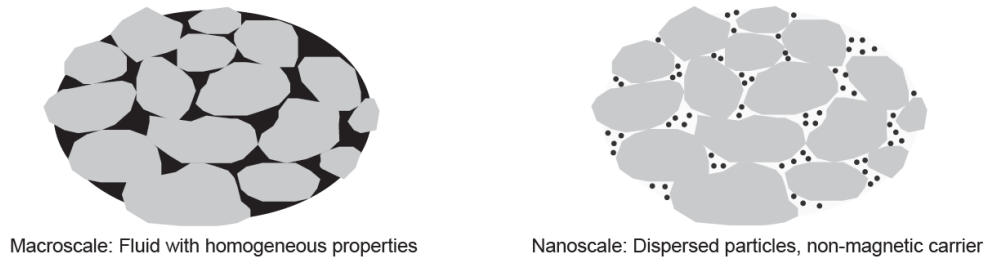
evaluated based on susceptibility changes, then the measured susceptibility is compared to the expected susceptibility computed as the product of pore space volume and initial susceptibility of the (diluted) ferrofluid. This would be an accurate estimate if the effective susceptibility of the fluid were equal to the initial susceptibility. However, when the effective susceptibility at measurement conditions deviates from the initial susceptibility used to estimate impregnation efficiency, the obtained results are misleading. The effective susceptibility of EMG705 at 1 kHz is ~35% of the initial susceptibility stated in the fluid's technical specifications. Thus, when the entire pore space is impregnated, but the difference between initial and effective susceptibility are not considered, the calculated impregnation efficiency (35%) would significantly underestimate the proportion of impregnated pore space. At the same time, when the effective susceptibility is higher than the initial susceptibility, the impregnation efficiency would be overestimated unless effective susceptibilities are used in the calculation. For EMG909, impregnation of 66-80% of the pore space seemingly leads to an impregnation efficiency of 100%, when it is calculated based on the fluid's initial susceptibility. This may lead to the wrong conclusion that oil-based ferrofluid is more efficient at impregnating rock samples, and different ways of characterizing impregnation efficiency should be used in combination. In fact, oil-based ferrofluid has been described as more efficient at impregnation than water-based fluid, but based on weight changes (Robion *et al.*, 2014).

#### 4.4 Artefacts and recommendations for sample preparation

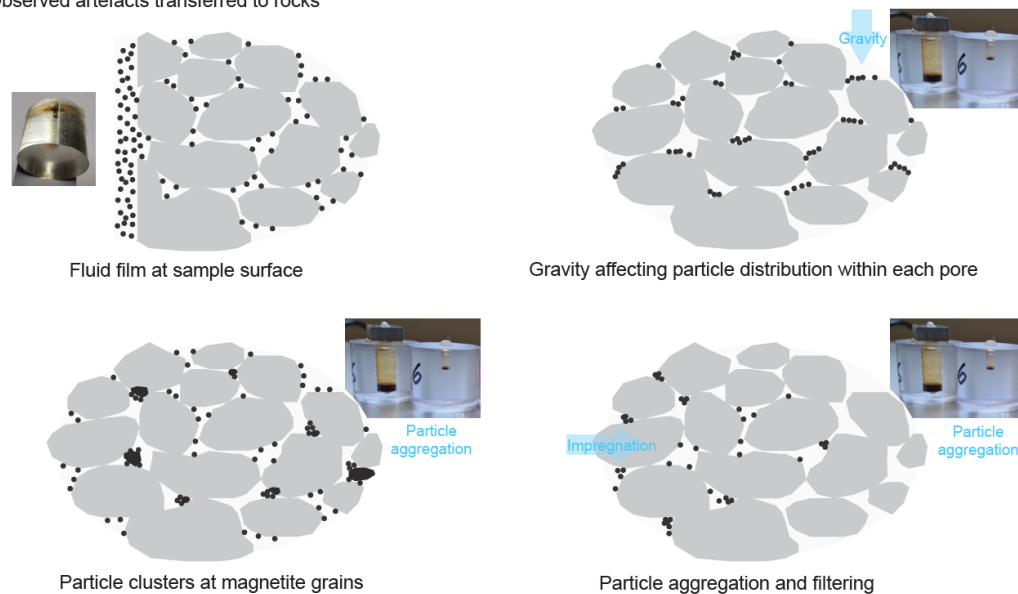
In addition to providing explanations for the large variability in published empirical relationships, the data presented here also give insight into some of the challenges that arise from working with colloidal suspensions rather than solid magnetite grains in rock samples. These include (1) the fluid not occupying the supposed space or moving out of that space after preparation, during the measurement or during storage, (2) trapping of air, (3) aggregation of the particles in the fluid, so that the susceptibility and magnetization vary within the fluid-occupied space. Some of these are specifically related to the type of synthetic samples investigated here, but others are more related to

the fluid itself, and we will discuss how the observed artefacts may manifest in rocks, and formulate some recommendations for studies on impregnated rock samples (Fig. 12).

(a) Ideal distribution of ferrofluid



(b) Observed artefacts transferred to rocks



(c) Related challenges to be investigated in rocks

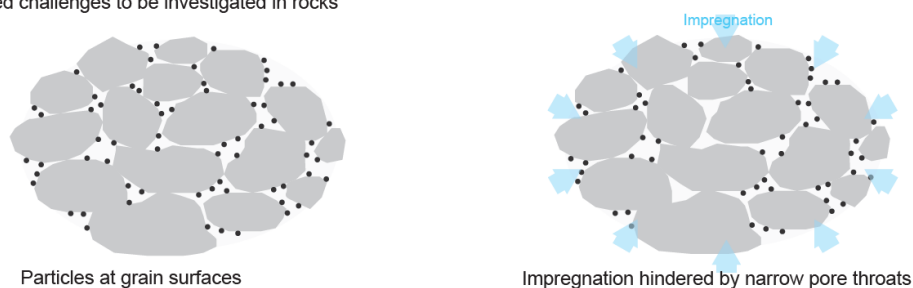


*Fig. 12: (a) Ideal distribution of ferrofluid in a rock's pore space on the macroscale (homogeneous fluid, used for modelling MPFs) and nanoscale (dispersed magnetic nanoparticles in non-magnetic carrier fluid). (b) Conceptual sketches of how the artefacts observed in synthetic samples may transfer to rocks: Fluid at the sample-seal interface could translate to a film of ferrofluid at the sample surface; particle aggregation and sedimentation could translate to gravity affecting the distribution of nanoparticles within each pore, nanoparticles clustering around magnetite grains in the rock, or particle aggregation and filtering effects during the impregnation process. (c) Related challenges that may occur in rocks include particles clustering at grain surfaces, rather than being*

*distributed uniformly throughout the pore space, or parts of the pore space not being impregnated due to bottlenecks at narrow pore throats, again resulting in a non-uniform distribution of magnetic particles throughout the pore space.*

Magnetic pore fabrics in rocks are interpreted assuming that the entire pore space is filled with a homogeneous fluid of constant susceptibility. On the nanoscale, this corresponds to a random distribution of the magnetic nanoparticles throughout the pore space (Fig. 12a). A major issue we observe in our synthetic samples is ferrofluid moving out of the voids and migrating along the interface of the seal (tape, glue, plastic plate) and the sample cylinder, with the result that air bubbles form inside the voids (cf. Fig. 3). This appears especially important for oil-based fluid that destroyed all our seals over time. The migrated fluid at the interface naturally possesses strong anisotropy as it is constrained by two flat surfaces in contact with each other. The strong shape anisotropy of a small amount of migrated fluid may outweigh the weaker anisotropy of the fluid inside the void, and thus dominate the measurements. Similarly, a film of ferrofluid on the surface of a rock sample could significantly affect the measured MPF (Fig. 12b). This is especially problematic when the sample is wrapped in e.g. plastic, which is advisable to protect the instrument from contamination. Parés *et al.* (2016) encapsulated their samples in plastic boxes, preventing them from touching the walls using plastic spacers, to minimize buildup of a fluid film. Alternative approaches may include advanced sealing of surface pores, e.g. using varnish, or the evaporation of the carrier fluid after impregnation, to immobilize the particles. Surface effects are less prominent in larger samples that have the additional advantage of being more representative of the rock volume. However, large samples are harder to impregnate, so that smaller samples are preferred in MPF studies (Almqvist *et al.*, 2011, Parés *et al.*, 2016). Therefore, the selection of sample size will always be a compromise between impregnation efficiency and the reduction of surface artefacts.

The air replacing the fluid in the synthetic samples diminishes the anisotropy of the fluid in the void, as it decreases its aspect ratio. This effect was especially relevant for voids of small volume, i.e., the

ZK3, ZK4 and D05 series. Trapped air within the void can also move during a measurement, and be located at different positions for each measurement direction. If this happens, different fluid shapes and thus shape anisotropies are measured in each direction and that data should strictly not be used to calculate one common anisotropy tensor. Some air bubbles moved during sample storage (cf Fig. 3). In rocks, trapped air may block entry to some pores, thus diminishing impregnation efficiency, and if located in larger pores, cause deviations between the fluid distribution and the pore space. It is possible for example, that gravity causes all nanoparticles, especially when aggregated, to concentrate at the bottom of each pore, while air is located at the top of the pores. This inhomogeneous particle and susceptibility distribution would affect the measured magnetic anisotropy. More work is needed to investigate the distribution of the magnetite particles within a single pore or throughout the pore space, and reduce these artefacts.

Particle aggregation and sedimentation is another process that leads to inhomogeneous distribution of susceptibility and magnetization throughout the fluid, and may further affect the magnetic properties due to increased interaction between particles. We have mainly seen aggregation in the oil-based EMG909 ferrofluid at the lowest concentration used (1:50), leading to measured anisotropies opposite to the shape of the void. This is important in light of previous studies that used even lower concentrations of 1:100 to avoid saturating the signal of the susceptibility meter (Parés *et al.*, 2016), and who favoured oil-based ferrofluid over water-based ferrofluid due to its better impregnation properties (Robion *et al.*, 2014). A careful evaluation of impregnation properties, instrument capabilities and potential artefacts is necessary prior to choosing the most appropriate ferrofluid. In rocks, particles may not only aggregate with each other, but could cluster at magnetite grains, or other minerals with high susceptibility. Due to their larger diameter, particle aggregates will have more difficulties migrating through narrow pore throats and impregnating small pores, decreasing the number of pores that are reached, and diminishing the resolution and usefulness of the MPF method. Our results illustrate that higher fluid susceptibilities lead to stronger anisotropies,

and that higher concentrations and water-based fluids may be less prone to particle aggregation compared to lower concentrations and oil-based fluids.

Additional challenges that may arise in rocks, but are not observed here in the synthetic samples are that particles may be concentrated at the grain surfaces rather than distributed throughout the pores, and that impregnation may be hindered in parts of the sample due to narrow pore throats (Fig. 12c). The latter is particularly important when particles are aggregated and thus larger than the nominal 10 nm diameter. Incomplete impregnation in the core of the sample is a recurring issue in MPF studies (Almqvist *et al.*, 2016; Robion *et al.*, 2014). Parés *et al.* (2016) have prepared smaller samples to overcome this issue. Additional characteristics of the rock, including pore tortuosity and wettability of the minerals, which are known to affect fluid flow (Abdallah *et al.*, 2007; Clennell, 1997; Ghanbarian *et al.*, 2013), will also affect the impregnation process.

Note that the quality of the magnetic data, as defined by confidence ellipses and F-statistics (Hext, 1963, Jelinek, 1977) or  $R_1$  values from repeat measurements (Biedermann *et al.*, 2013), provides no information on the presence or severity of any of these artefacts. Here, artefacts could be identified from deviations between models and measurements, e.g. for the D05 samples, and because the synthetic samples are transparent, the trapped air and migrated fluid along the sample-seal interface are observed. It remains to be investigated how important similar artefacts are in rocks, where they are not as easily identifiable. Most of these artefacts seem to worsen over time, so that we would generally recommend to measure MPFs right after sample impregnation for best results.

## 5. Conclusions

This study investigated the magnetic susceptibility and anisotropy of ferrofluid-filled voids in synthetic samples. Computations of shape and distribution anisotropies were compared to low-field AMS measured at different frequencies. The measured anisotropy of voids filled with EMG705 water-based ferrofluid is generally lower than that predicted by models based on the initial susceptibility of the fluid, and decreases with increasing measurement frequency. For EMG909 oil-



based fluid, the measurements agree more closely with the models, and there is a weaker frequency-dependence. These observations can be explained by shape anisotropy being a function of the fluid's effective intrinsic susceptibility, which shows a strong frequency-dependence for EMG705, and weaker frequency-dependence for EMG909.

For a single pore of a given shape, the measured degree of magnetic anisotropy increases nonlinearly with the fluid susceptibility. The effective intrinsic fluid susceptibility depends on the type of ferrofluid and its concentration, and the measurement frequency. This frequency-dependence is important to take into account when defining and interpreting empirical relationships between the MPF anisotropy degree and pore aspect ratios. Analogously, the fluid properties and measurement conditions affect empirical relationships between MPF and permeability anisotropy, and may complicate the determination and comparison of impregnation efficiency between different fluids.

The details of the frequency-dependence vary between the two ferrofluids used here, EMG705 and EMG909. It is possible that other oil-based ferrofluids have a similar frequency-dependence as EMG909, and other water-based fluids behave analogously to EMG705, but it is also possible that each fluid displays its own frequency-dependence. Hence, the initial susceptibilities as specified by the manufacturer do not reflect the effective susceptibilities at measurement conditions, and there is no universally applicable relationship between initial and effective susceptibilities. These findings may explain in part or full the variability of reported empirical relationships. We therefore recommend that measurement frequencies, and frequency-dependence of susceptibilities are reported in future MPF studies, in addition to ferrofluid type and concentration. Detailed information on magnetic properties of ferrofluids at actual measurement conditions of MPF studies will help correct for frequency-related variations in MPF parameters, facilitating the comparison between empirical relationships reported in different studies. The results shown here present an important step towards a quantitative and robust interpretation of MPF data in terms of pore fabric

properties or permeability anisotropy. Thus, we believe that the method is more applicable to fluid migration studies in the future, facilitating the characterization of reservoirs and aquifers, and supporting convective flow, geothermal energy and CO<sub>2</sub> sequestration applications.

Higher effective intrinsic susceptibilities enable the description of weak pore fabrics, and simplify the distinction between different fabric strengths. Optimal parameters can be achieved by selecting the appropriate type and concentration of ferrofluid, as well as measurement frequency. A final recommendation for future MPF studies is related to the migration of fluid and particle aggregation that occur over time. Translated to rocks, these processes may cause artefacts leading to erroneous pore fabric interpretation, including formation of a film of ferrofluid on the sample surface or between the sample surface and sample holder, aggregation of particles inside pores, clustering of nanoparticles at magnetite grains, or filtering effects during impregnation. To avoid these artefacts, we consider it best to measure MPFs within a few days after impregnation.

## Acknowledgements

Sandro Bula and Thomas Siegenthaler, Institute of Geological Sciences, University of Bern, and Georges Schwyzer, Physics Institute, University of Bern, are gratefully acknowledged for preparing the samples. Magnetic measurements were performed at the Laboratory of Natural Magnetism at ETH Zurich, and we are grateful for access to the laboratory. Constructive and detailed reviews by Josep Parés and Philippe Robion helped to improve the manuscript. We thank Eduard Petrovsky for handling the manuscript. This study was funded by the Swiss National Science Foundation, project 176917.

## Data Availability

All data is reported in the paper and supplementary materials. The FinlrrSDA model used here for the predictions has been previously published (Biedermann, 2020), and the code is available on <https://zenodo.org/record/4040785>.

## References

- Abdallah, W., Buckley, J.S., Carnegie, A., Edwards, J., Herold, B., Fordham, E., Graue, A., Habashy, T., Seleznev, N., Signer, C., Hussain, H., Montaron, B., Ziauddin, M., 2007. Fundamentals of wettability. *Oilfield Review* 19, 44-61.
- Almqvist, B.S.G., Mainprice, D., Madonna, C., Burlini, L. & Hirt, A.M., 2011. Application of differential effective medium, magnetic pore fabric analysis, and X-ray microtomography to calculate elastic properties of porous and anisotropic rock aggregates, *Journal of Geophysical Research-Solid Earth*, 116.

- Ayan, C., Colley, G., Ezekwe, E., Wannell, M., Goode, P., Halford, F., Joseph, J., Mongini, A., Obondoko, G. & Pop, J., 1994. Measuring permeability anisotropy: The latest approach, *Oilfield Review*, 6, 24-35.
- Bean, C.P. & Livingston, J.D., 1959. Superparamagnetism, *Journal of Applied Physics*, 30, S120-S129.
- Benson, P.M., Meredith, P.G. & Platzman, E.S., 2003. Relating pore fabric geometry to acoustic and permeability anisotropy in Crab Orchard Sandstone: A laboratory study using magnetic ferrofluid, *Geophysical Research Letters*, 30, 1976.
- Biedermann, A.R., 2019. Magnetic pore fabrics: the role of shape and distribution anisotropy in defining the magnetic anisotropy of ferrofluid-impregnated samples, *Geochemistry, Geophysics, Geosystems*, 20, 5650-5666.
- Biedermann, A.R., 2020. FinIrrSDA: A 3D model for magnetic shape and distribution anisotropy of finite irregular arrangements of particles with different sizes, geometries, and orientations, *Journal of Geophysical Research: Solid Earth*, e2020JB020300.
- Biedermann, A.R., Lowrie, W. & Hirt, A.M., 2013. A method for improving the measurement of low-field magnetic susceptibility anisotropy in weak samples, *Journal of Applied Geophysics*, 88, 122-130.
- Brown, W.F., 1959. Relaxational Behavior of Fine Magnetic Particles, *Journal of Applied Physics*, 30, S130-S132.
- Brown, W.F., 1963. Thermal Fluctuations of a Single-Domain Particle, *Physical Review*, 130, 1677-1686.
- Cañón-Tapia, E., 1996. Single-grain versus distribution anisotropy: a simple three-dimensional model, *Physics of the Earth and Planetary Interiors*, 94, 149-158.
- Cañón-Tapia, E., 2001. Factors affecting the relative importance of shape and distribution anisotropy in rocks: theory and experiments, *Tectonophysics*, 340, 117-131.
- Clark, D.A., 2014. Methods for determining remanent and total magnetisations of magnetic sources – a review. *Exploration Geophysics*, 45, 271-304.
- Clark, D.A. & Emerson, D.W., 1999. Self-Demagnetisation, *Preview*, 79, 22-25.
- Clennell, M.B., 1997. Tortuosity: a guide through the maze. In: Lovell, M.A., Harvey, P.K. (ed.) *Developments in Petrophysics, Geological Society of London Special Publication*, 122, 299-344.
- Cnudde, V. & Boone, M.N., 2013. High-resolution X-ray computed tomography in geosciences: A review of the current technology and applications, *Earth-Science Reviews*, 123, 1-17.
- Coffey, W.T. & Kalmykov, Y.P., 2012. Thermal fluctuations of magnetic nanoparticles: Fifty years after Brown, *Journal of Applied Physics*, 112.
- Dearing, J.A., Dann, R.J.L., Hay, K., Lees, J.A., Loveland, P.J., Maher, B.A. & O'Grady, K., 1996. Frequency-dependent susceptibility measurements of environmental materials, *Geophysical Journal International*, 124, 228-240.
- Dormann, J.L., 1981. Le phénomène de superparamagnétisme, *Revue de Physique Appliquée*, 16, 275-301.
- Esteban, L., Géraud, Y. & Bouchez, J.L., 2006. Pore network geometry in low permeability argillites from magnetic fabric data and oriented mercury injections, *Geophysical Research Letters*, 33, L18311.
- Eyre, J.K., 1997. Frequency dependence of magnetic susceptibility for populations of single-domain grains, *Geophysical Journal International*, 129, 209-211.
- Ghanbarian, B., Hunt, A.G., Ewing, R.P., Sahimi, M., 2013. Tortuosity in porous media: a critical review. *Soil Science Society of America Journal*, 77, 1461-1477.
- Goya, G.F., Berquó, T.S., Fonseca, F.C. & Morales, M.P., 2003. Static and dynamic magnetic properties of spherical magnetite nanoparticles, *Journal of Applied Physics*, 94, 3520-3528.
- Grégoire, V., Darrozes, P., Gaillot, P. & Nédélec, A., 1998. Magnetite grain shape fabric and distribution anisotropy vs rock magnetic fabric: a three-dimensional case study, *Journal of Structural Geology*, 20, 937-944.

Grégoire, V., De Saint-Blanquat, M., Nédélec, A. & Bouchez, J.-L., 1995. Shape anisotropy versus magnetic interactions of magnetite grains: experiments and application to AMS in granitic rocks, *Geophysical Research Letters*, 22, 2765-2768.

Hailwood, E.A., Bowen, D., Ding, F., Corbett, P.W.M. & Whattler, P., 1999. Characterizing pore fabrics in sediments by anisotropy of magnetic susceptibility analyses. in *Paleomagnetism and Diagenesis in Sediments*, pp. 125-126, eds. Tarling, D. H. & Turner, P. Geological Society, London, Special Publications.

Hailwood, E. & Ding, F., 2000. Sediment transport and dispersal pathways in the Lower Cretaceous sands of the Britannia Field, derived from magnetic anisotropy, *Petroleum Geoscience*, 6, 369-379.

Hargraves, R.B., Johnson, D. & Chan, C.Y., 1991. Distribution anisotropy: the cause of AMS in igneous rocks?, *Geophysical Research Letters*, 18, 2193-2196.

Hext, G.R., 1963. The estimation of second-order tensors, with related tests and designs, *Biometrika*, 50, 353-373.

Hrouda, F., 2011. Models of frequency-dependent susceptibility of rocks and soils revisited and broadened, *Geophysical Journal International*, 187, 1259-1269.

Hrouda, F., Chadima, M., Jezek, J. & Pokorný, J., 2017. Anisotropy of out-of-phase magnetic susceptibility of rocks as a tool for direct determination of magnetic subfabrics of some minerals: an introductory study, *Geophysical Journal International*, 208, 385-402.

Hrouda, F., Hanak, J. & Terzijski, I., 2000. The magnetic and pore fabrics of extruded and pressed ceramic models, *Geophysical Journal International*, 142, 941-947.

Hrouda, F., Pokorný, J. & Chadima, M., 2015. Limits of out-of-phase susceptibility in magnetic granulometry of rocks and soils, *Studia Geophysica et Geodaetica*, 59, 294-308.

Hrouda, F., Pokorný, J., Ježek, J. & Chadima, M., 2013. Out-of-phase magnetic susceptibility of rocks and soils: a rapid tool for magnetic granulometry, *Geophysical Journal International*, 194, 170-181.

Huang, T., Tao, Z., Li, E., Lyu, Q. & Guo, X., 2017. Effect of permeability anisotropy on the production of multi-scale shale gas reservoirs, *Energies*, 10.

Humbert, F., Robion, P., Louis, L., Bartier, D., Ledésert, B. & Song, S.-R., 2012. Magnetic inference of in situ open microcracks in sandstone samples from the Taiwan Chelungpu Fault Drilling Project (TCDP), *Journal of Asian Earth Sciences*, 45, 179-189.

Ijeje, J.J., Gan, Q. & Cai, J., 2019. Influence of permeability anisotropy on heat transfer and permeability evolution in geothermal reservoir, *Advances in Geo-Energy Research*, 3, 43-51.

Jackson, M., 2003-2004. Imaginary Susceptibility - A Primer, *The IRM Quarterly*, 13, 1, 10-11.

Jackson, M., Moskowitz, B., Rosenbaum, J. & Kissel, C., 1998. Field-dependence of AC susceptibility in titanomagnetites, *Earth and Planetary Science Letters*, 157, 129-139.

Jelinek, V., 1977. The statistical theory of measuring anisotropy of magnetic susceptibility of rocks and its application.

Jelinek, V., 1981. Characterization of the magnetic fabric of rocks, *Tectonophysics*, 79, T63-T67.

Jezek, J. & Hrouda, F., 2007. A program for magnetic susceptibility-equivalent pore conversion, *Geochemistry Geophysics Geosystems*, 8, GC001709.

Jones, D.H. & Srivastava, K.K.P., 1989. A re-examination of models of superparamagnetic relaxation, *Journal of Magnetism and Magnetic Materials*, 78, 320-328.

Jones, S., Benson, P. & Meredith, P., 2006. Pore fabric anisotropy: testing the equivalent pore concept using magnetic measurements on synthetic voids of known geometry, *Geophysical Journal International*, 166, 485-492.

Joseph, A. & Mathew, S., 2014. Ferrofluids: synthetic strategies, stabilization, physicochemical features, characterization, and applications, *ChemPlusChem*, 79, 1382-1420.

Joseph, R.I., 1966. Ballistic demagnetizing factor in uniformly magnetized cylinders, *Journal of Applied Physics*, 37, 4639-4643.

942 Joseph, R.I., 1967. Ballistic demagnetizing factor in uniformly magnetized rectangular prisms, *Journal*  
943 *of Applied Physics*, 38, 2405-2406.

944 Joseph, R.I., 1976. Demagnetizing factors in nonellipsoidal samples - a review, *Geophysics*, 41, 1052-  
945 1054.

946 Joseph, R.I. & Schlömann, E., 1965. Demagnetizing field in nonellipsoidal bodies, *Journal of Applied*  
947 *Physics*, 36, 1579-1593.

948 Kosterov, A.A., Sergienko, E.S., Kharitonskii, P.V. & Yanson, S.Y., 2018. Low temperature magnetic  
949 properties of basalts containing near ~TM30 titanomagnetite, *Izvestiya, Physics of the Solid*  
950 *Earth*, 54, 134-149.

951 Landis, E.N. & Keane, D.T., 2010. X-ray microtomography, *Materials Characterization*, 61, 1305-1316.

952 Louis, L., David, C., Metz, V., Robion, P., Menendez, B. & Kissel, C., 2005. Microstructural control on  
953 the anisotropy of elastic and transport properties in undeformed sandstones, *International*  
954 *Journal of Rock Mechanics and Mining Sciences*, 42, 911-923.

955 Muscas, G., Concas, G., Cannas, C., Musinu, A., Ardu, A., Orrù, F., Fiorani, D., Laureti, S., Rinaldi, D.,  
956 Piccaluga, G. & Peddis, D., 2013. Magnetic Properties of Small Magnetite Nanocrystals, *The*  
957 *Journal of Physical Chemistry C*, 117, 23378-23384.

958 Nabawy, B.S., Rochette, P. & Géraud, Y., 2009. Petrophysical and magnetic pore network anisotropy  
959 of some cretaceous sandstone from Tushka Basin, Egypt, *Geophysical Journal International*,  
960 177, 43-61.

961 Néel, L., 1949. Influence des fluctuations thermiques sur l'aimantation de grains ferromagnétiques  
962 très fins, *Comptes rendus hebdomadaires des séances de l'Académie des sciences* T228, 664-  
963 666.

964 Odenbach, S., 2004. Recent progress in magnetic fluid research, *Journal of Physics: Condensed*  
965 *Matter*, 16, R1135-R1150.

966 Osborn, J.A., 1945. Demagnetizing factors of the general ellipsoid, *Physical Review*, 67, 351-357.

967 Panja, P., McLennan, J. & Green, S., 2021. Influence of permeability anisotropy and layering on  
968 geothermal battery energy storage, *Geothermics*, 90.

969 Papaefthymiou, G.C., 2009. Nanoparticle magnetism, *Nano Today*, 4, 438-447.

970 Parés, J., Miguens, L. & Saiz, C., 2016. Characterizing pore fabric in sandstones with magnetic  
971 anisotropy methods: initial results, *Journal of Petroleum Science and Engineering*, 143, 113-  
972 120.

973 Pfeleiderer, S. & Halls, H.C., 1990. Magnetic susceptibility anisotropy of rocks saturated with  
974 ferrofluid: a new method to study pore fabric?, *Physics of the Earth and Planetary Interiors*,  
975 65, 158-164.

976 Pfeleiderer, S. & Halls, H.C., 1993. Magnetic pore fabric analysis: Verification through image  
977 autocorrelation, *Journal of Geophysical Research*, 98, 4311-4316.

978 Pfeleiderer, S. & Halls, H.C., 1994. Magnetic pore fabric analysis: a rapid method for estimating  
979 permeability anisotropy, *Geophysical Journal International*, 116, 39-45.

980 Pfeleiderer, S. & Kissel, C., 1994. Variation of pore fabric across a fold-thrust structure, *Geophysical*  
981 *Research Letters*, 21, 2147-2150.

982 Pugnetti, M., Zhou, Y., Biedermann, A.R., 2021 Experimental improvements for ferrofluid  
983 impregnation of rocks using directional forced impregnation methods: results on natural and  
984 synthetic samples. EGU virtual general assembly.

985 Robion, P., David, C., Dautriat, J., Colombier, J.-C., Zinsmeister, L. & Collin, P.-Y., 2014. Pore fabric  
986 geometry inferred from magnetic and acoustic anisotropies in rocks with various  
987 mineralogy, permeability and porosity, *Tectonophysics*, 629, 109-122.

988 Rosensweig, R.E., 1987. Magnetic fluids, *Annual Review of Fluid Mechanics*, 19, 437-463.

989 Rosensweig, R.E., 1988. An introduction to ferrohydrodynamics, *Chemical Engineering*  
990 *Communications*, 67, 1-18.

991 Sato, M. & Ishii, Y., 1989. Simple and approximate expressions of demagnetizing factors of uniformly  
992 magnetized rectangular rod and cylinder, *Journal of Applied Physics*, 66, 983-985.

- Sinan, S., Glover, P.W.J. & Lorinczi, P., 2020. Modelling the impact of anisotropy on hydrocarbon production in heterogeneous reservoirs, *Transport in Porous Media*, 133, 413-436.
- Söffge, F. & Schmidbauer, E., 1981. AC susceptibility and static magnetic properties of an  $\text{Fe}_3\text{O}_4$  ferrofluid, *Journal of Magnetism and Magnetic Materials*, 24, 54-66.
- Stephenson, A., 1971. Single domain grain distributions: 1. A method for the determination of single domain grain distributions, *Physics of the Earth and Planetary Interiors*, 4, 353-360.
- Stephenson, A., 1994. Distribution anisotropy: two simple models for magnetic lineation and foliation, *Physics of the Earth and Planetary Interiors*, 82, 49-53.
- Stoner, E.C., 1945. The demagnetizing factors for ellipsoids, *The London, Edinburgh, and Dublin Philosophical Magazine and Journal of Science: Series 7*, 36, 803-821.
- Storesletten, L., 1998. Effects of anisotropy on convective flow through porous media. in *Transport Phenomena in Porous Media*, pp. 261-283, eds. Ingham, D. B. & Pop, I. Pergamon (Elsevier), Oxford, UK.
- Syono, Y., 1965. Magnetocrystalline anisotropy and magnetostriction of  $\text{Fe}_3\text{O}_4$ - $\text{Fe}_2\text{TiO}_4$  series, with special application to rock magnetism, *Japanese Journal of Geophysics*, 4, 71-143.
- Torres-Diaz, I. & Rinaldi, C., 2014. Recent progress in ferrofluids research: novel applications of magnetically controllable and tunable fluids, *Soft Matter*, 10, 8584-8602.
- Wang, C., Huang, Z., Lu, Y., Tang, G. & Li, H., 2019. Influences of reservoir heterogeneity and anisotropy on  $\text{CO}_2$  sequestration and heat extraction for  $\text{CO}_2$ -based enhanced geothermal system, *Journal of Thermal Science*, 28, 319-325.
- Wang, G., Wei, X., An, H., Wang, F.-Y. & Rudolph, V., 2014. Modeling anisotropic permeability of coal and its effects on coalbed methane reservoir simulation. in *Proceedings of the 4th International Conference on Simulation and Modeling Methodologies, Technologies and Applications*, pp. 477-483.
- Willems, C.J.L., Nick, H.M., Donselaar, M.E., Weltje, G.J. & Bruhn, D.F., 2017. On the connectivity anisotropy in fluvial Hot Sedimentary Aquifers and its influence on geothermal doublet performance, *Geothermics*, 65, 222-233.
- Worm, H.-U., 1998. On the superparamagnetic - stable single domain transition for magnetite, and frequency dependence of susceptibility, *Geophysical Journal International*, 133, 201-206.
- Worm, H.-U. & Jackson, M., 1999. The superparamagnetism of Yucca Mountain Tuff, *Journal of Geophysical Research: Solid Earth*, 104, 25415-25425.
- Zhou, Y., Pugnetti, M., Foubert, A., Lanari, P., Neururer, C., Biedermann, A.R., 2021. Correlations of magnetic pore fabrics with pore fabrics derived from high-resolution X-ray computed tomography and with permeability anisotropy in sedimentary rocks and synthetic samples. EGU virtual general assembly.